www.sciencemag.org/content/352/6287/828/suppl/DC1

Supplementary Materials for

Fusion peptide of HIV-1 as a site of vulnerability to neutralizing antibody

Rui Kong, Kai Xu, Tongqing Zhou, Priyamvada Acharya, Thomas Lemmin, Kevin Liu, Gabriel Ozorowski, Cinque Soto, Justin D. Taft, Robert T. Bailer, Evan M. Cale, Lei Chen, Chang W. Choi, Gwo-Yu Chuang, Nicole A. Doria-Rose, Aliaksandr Druz, Ivelin S. Georgiev, Jason Gorman, Jinghe Huang, M. Gordon Joyce, Mark K. Louder, Xiaochu Ma, Krisha McKee, Sijy O'Dell, Marie Pancera, Yongping Yang, Scott C. Blanchard, Walther Mothes, Dennis R. Burton, Wayne C. Koff, Mark Connors, Andrew B. Ward, Peter D. Kwong,* John R. Mascola*

*Corresponding author. Email: pdkwong@nih.gov (P.D.K); jmascola@nih.gov (J.R.M.)

Published 13 May 2016, *Science* **352**, 828 (2016)
DOI: 10.1126/science.aae0474

This PDF file includes:

Other Supplementary Material for this manuscript includes the following:
(available at www.sciencemag.org/cgi/content/full/352/6287/828/DC1)

Databases S1 to S3 as Excel files

Materials and Methods

Human specimens

The sera and peripheral blood mononuclear cells (PBMCs) used in this study were collected from donor N123 on June 22nd, 2009. This donor is a chronically HIV-1-infected individual enrolled in the National Institute of Allergy and Infectious Disease (NIAID) under a clinical protocol approved by the NIAID Investigational Review Board (*8, 9*). This donor was diagnosed with HIV in 2000. After more than nine years of infection, this donor showed a CD4 T-cells count of 463 cells/ml and a plasma HIV-1 viral load of 4920 RNA copies/ml at the time of sample collection. This donor was not on antiretroviral treatment. Other 23 sera tested in this study were also from chronically HIV-1 infected subjects enrolled in the NIAID cohort. As described previously (*8, 9*), all the donors were presumed to be infected with clade B virus based on the locations of current and former residences.

HIV-1 Env-pseudotyped virus

HIV-1 Env-pseudotyped virus stocks were grown in 293T cells by cotransfection of a pSG3ΔEnv backbone and an Env expression plasmid as described (*40*). To produce virus stocks with glycosylation modifications, virus stocks were grown in 293T cells in the presence of glycosylation inhibitor kifunensine at 25 μM, or in the presence of swainsonine at 20 μM, or GNTI-/- 293S cells as described (*11, 13*).

Neutralization assays

Serum and monoclonal antibodies (mAbs) neutralization was assessed in a single round virus infection assay using TZM-bl target cells (TZM-bl assay) as described (*40*). The serum was assayed at 8-point 4-fold dilutions starting at 1:100 dilutions, and the mAbs were assayed at 5-fold dilutions starting at 50 μg/ml. A nonlinear regression neutralization curve was fit using 5-parameter hill slope equation, and the 50% and 80% inhibitory concentrations (IC_{50} and IC_{80}) were determined. To evaluate the neutralizing activity of mAb N123-VRC34.01 on a panel of 208 HIV-1 strains, an automated 384-well microneutralization assay was performed as described (*41, 42*).

To evaluate the interaction of VRC34.01 with cell-free virus and the contribution of this interaction to neutralization, a washing step was introduced as described (*21, 43*). Briefly, JR-FL.JB pseudotyped virus stock (1:16 diluted) was mixed with 5-fold serially diluted mAbs. After 30 minutes incubation in 37 degrees, the virus-antibody mixture was centrifuged 40000 rpm for 20 minutes and the supernatant were discarded. Additional two washes were performed using cDMEM. Virus pellet was then resuspended into 500 μl cDMEM and 50 μl of which was mixed with 20 μl of TZM-bl cells (0.5 million/ml) for overnight incubation in 37 degrees. 130 μl cDMEM was added on day 2. On day 3, cells were lysed and the luciferase activity was measured as described (*21, 43*).

In neutralization competition assay, 5 μl of protein or medium was added to each well including cell-only and virus-only control wells at a concentration of 250 μg/ml. 10 μl of 5-fold serially diluted mAbs or 4-fold serially diluted human sera were then added. The protein/antibody mixture was incubated for 30 minutes at 37 °C before adding 35 μl

of viruses. The final concentration of the protein in the 50 µl mixture is 25 µg/ml. The starting concentration of mAbs in the mixture is 50 µg/ml, and the starting concentration of human sera is 1:20. The mixture was further incubated for 30 minutes at 37 °C before adding 20 µl of TZM-bl cells (0.5 million/ml). After overnight incubation at 37 °C, 130 µl cDMEM was added. On day 3, cells were lysed and the luciferase activity was measured.

Serum neutralization fingerprint analysis

The epitope specificity of donor N123 serum was predicted using neutralization fingerprint analysis (*44*). Briefly, the serum neutralization on a panel of 21 HIV-1 strains was determined by TZM-bl assay. The polyclonal serum neutralization fingerprint, i.e. the pattern of neutralization titers, was represented as a combination of the neutralization fingerprints of a reference set of mAbs targeting the main sites of vulnerability on HIV-1 Env. The score of each reference mAb specificity was determined based on the method described previously (*44*), and then used to predict the polyclonal serum specificity. The fingerprinting method, due to its underlying mathematical constraints (*44*), must distribute the scores to the set of reference antibody specificities, and is thus not optimal for use in cases where the sera include dominant specificities not found in the reference set.

Probe production, memory B cell sorting and Ig gene recovery

The trimeric HIV-1 Env BG505 SOSIP.664.T332N gp140 with an Avi tag (GLNDIFEAQKIEWHE) inserted at the C-terminus was expressed and purified as described (*45*). Briefly, the BG505 SOSIP.664.T332N and furin plasmid DNAs were co-transfected into 293F cells. The supernatants were harvested 6 days post transfection, and purified through VRC01 antibody –affinity column followed by gel filtration. The BG505 SOSIP.664.T332N protein was further biotinylated using birA ligase (Avidity) and conjugated to streptavidin-PE (Invitrogen) as described (*40*).

PBMCs (6/22/09) from donor N123 were stained using LIVE/DEAD® Fixable Aqua (Invitrogen); CD3-Cy7APC, CD4-BV605, CD14-BV605, CD8-BV711, CD19-Cy7PE, IgG-Alx680 and IgM-Cy5PE (BD Pharmingen). They were also stained with probe BG505 SOSIP.664.T332N-streptavidin-PE. Cells that were CD3-CD4-CD14-CD8-CD19+IgG+IgM- and BG505 SOSIP-streptavidin-PE+ were sorted into 96-well plates at single cell per well using a BD Aria II as described (*40*). The variable regions of gamma, kappa and lambda chain genes were recovered from singe B cell as described (*40*). Briefly, RT-PCR was performed using single cell lysate. Nested PCR were than performed to amplify heavy or light chain genes using different multiplex primer pools as described (*45*). PCR products were sequenced, analyzed using IMGT database (http://www.imgt.org/) and then subcloned into expression vectors. Paired heavy and light chain genes were then co-expressed and purified to obtain monoclonal antibodies as described (*40*).

ELISA

BG505 gp120 ELISA and VRC34-epitope scaffold ELISA was performed as described (*40*). Briefly, plates were coated with protein overnight at 4 °C. Coated plates

were blocked, incubated with serially diluted antibody or serum, and then incubated with goat anti-human IgG conjugated with horseradish peroxidase (HRP) (Jackson ImmunoResearch Laboratories Inc., West Grove, PA). Plates were washed 6 times between each step. Plates were further developed using 3,3',5,5'-tetramethylbenzidine (TMB) (Kirkegaard & Perry Laboratories) and read at 450 nM. For BG505 SOSIP.664 trimer ELISA, plates were coated with 2 μg/ml of a sheep anti-gp120 C5 antibody, D7324 capture antibody (Cliniqa Corp., Fallbrook, CA) in PBS overnight at 4 °C. Plates were then blocked with 200 μl/well of 5% milk in PBS for 1 hour at 37 °C, followed by incubation with BG505 SOSIP.664 trimer with D7324 tag at 2 μg/ml in 10% PBS for 2 hours at 37 °C. Plates were further incubated with first and antibody, and then developed as described above. For competition ELISA on BG505 SOSIP. 664 trimer, after the incubation with BG505 SOSIP.664 trimer with D7324 tag, 50 μl of cold competitor mAbs at 20 μg/ml was added to the plates and incubated for 15 minutes, and 50 ul of the biotinylated mAbs was added to the plates without washing. The final concentration of competitor mAbs was 10 μg/ml and the final concentration of biotinylated mAbs was pre-optimized by titration.

Cell surface staining

Cell surface staining was performed as described (*46*). Briefly, 293T cells were transfected by Env expression plasmids (JR-FL Env or BG505 Env). Cells were harvest 48 hours post transfection and stained with vivid staining buffer at room temperature for 30 min. Cells were washed using PBS and incubated with serially diluted mAbs for 30 min at room temperature. Cells were then washed and stained with mouse anti-human-IgG-PE. Cells were then fixed by resuspending in 150 μl 2%paraformaihehyde PBS and assessed by flow cytometry.

HIV-1 Env mutagenesis

Site-directed mutagenesis was performed on BG505 and Q23.17 Env through GeneImmune Biotechnology LLC, NY. Mutant Env plasmid was used to produce mutant Env-pseudotyped viruses.

FP sequence analysis

The sequence alignment of 3943 HIV-1 strains was downloaded from the HIV database (www.hiv.lanl.gov), and the frequency of different amino acid types at residue positions 512-519 was analyzed.

TZM-bl cell attachment assay

We tested the inhibition effect of mAbs on virus-cell attachment. 950 μl of JR-FL.JB pseudotyped viruses were mixed with 50 μl of mAbs (1 mg/ml) for a final concentration of 50 μg/ml or mixed with medium control, and then incubated at 37 degree for 30 minutes. 5 million TZM-bl cells were pelleted by centrifuging at 1000 rpm for 5 minutes and then resuspended in the virus-mAb mixture. After 30 minutes incubation at 37 degree, the cells were washed twice by PBS and resuspended in 150 μl vivid staining buffer for 30 minutes incubation at room temperature. After incubation, cells were washed twice with PBS and then incubated with biotinylated 2G12 for 30 minutes at room temperature. After that, cells were washed twice with PBS, and

incubated with streptavidin-PE for 30 minutes at room temperature. Finally, cells were washed twice with PBS and fixed by resuspending in 150 µl 2% paraformalhehyde PBS and assessed in flow cytometry. Median fluorescence intensity (MFI) was obtained from at least 10,000 cell events and background defined by the MFI of TZM-bl cells without virus incubation was subtracted from the MFI values. MFI values were then normalized to the medium control, in which no antibody was include; this was defined as 100%. Each experiment was repeated four times.

BG505 SOSIP.6R.664.T332N expression and purification

BG505SOSIP.6R.664 construct was synthesized as described previously, using BG505 genbank accession nos ABA61516 and DQ208458 (*47*), including the isoleucine to proline mutation at residue 559 (I559P), the SOS (A501C, T605C), the glycan site at residue 332 (T332N), mutating the cleavage site to 6R (REKR to RRRRR) and having the last residue being 664 per HX numbering.

The construct was cotranfected with furin in HEK 293 S GnTI-/- cells using 600 µgs plasmid DNA and 150 µgs of furin. The supernatants were harvested 7 days after transfection, and run over VRC01 affinity column. Following a PBS wash, the proteins were eluted using 3M $MgCl_2$, pH 7.4. The eluate was concentrated using centricon-70 and directly purified through Superdex 200 size exclusion chromatography in 5mM HEPES, pH 7.5, 150mM NaCl, 0.02% azide. The trimeric peak was isolated, concentrated and used directly or flash-frozen in liquid nitrogen and kept at -80°C until further use.

Fab expression and purification

PGT122 and VRC34.01 IgG were expressed as previously described. Heavy chain plasmids without (VRC34.01) or with (PGT122) HRV3C cleavage site in the hinge region were co-transfected with corresponding light chain plasmids in 293F or GnTI-/- (for PGT122 which is glycosylated) using TrueFect-Max transfection reagent (United Biosystems) according to manufacturer's protocol. Cultures were fed with fresh media 4 hours post-transfection and with enriched medium containing valproic acid (4mM final concentration) 24 hours after transfection. Cultures were then incubated at 33ºC for 6 more days and supernatants were harvested and passed though protein A column. After PBS wash and low pH elution, eluate was collected. Fabs were obtained by using either HRV3C cleavage (PGT122), or Lys-C (Roche) cleavage (VRC34.01) and Fabs were purified over superdex 200 column (GE) in 5mM HEPES, pH7.5, 150mM NaCl, 0.02% azide.

Complex preparation

PGT122 and VRC34.01 Fabs were added to a solution of purified BG505SOSIP.6R.664.T332N trimer in 2 fold molar excess for 30 min at RT. The complex was then partially deglycosylated by adding EndoH (1:10 v/v) in the gel filtration buffer and incubate overnight at 4°C. The complex was then purified over gel filtration and fractions were pooled, concentrated down to 8 mg/mL and used immediately for crystal screening or flash frozen in liquid nitrogen and kept at -80ºC until further use. Fusion peptide/VRC34.01 Fab complex was prepared by manually mixing

synthetic fusion peptide (residue 512 to 520, Genscript) and VRC34.01 Fab in 10:1 molar ratio.

Crystal screening

The VRC34.01 Fab only, ternary complex and Fusion peptide/VRC34.01 Fab complex were screened for crystallization using 572 conditions from Hampton, Wizard and Precipitant synergy screens using a Cartesian Honeybee crystallization robot as described previously (*48*) and a mosquito robot. Crystals were observed in a few conditions and were manually reproduced. VRC 34 crystal grew in 0.2M Zinc Acetate, 0.1M Sodium Cacodylate pH6.5 and 15% PEG 8000; The ternary complex crystals grew in 0.5M Sodium Chloride, 0.1M Tris-HCl pH8.5, 5% PEG 8000 and 20% 2-methyl-2, 4-pentanediol; Fusion peptide/VRC34.01 Fab complex crystal grew in 0.1M Imidazole pH8, 0.2M Calcium Acetate, 25% PEG 8000. The crystals were cryoprotected in 20% glycerol (for VRC34.01 Fab and fusion peptide/VRC34.01 Fab complex), or a solution of 30% Ethlene glycol (for ternary complex) and data were collected at a wavelength of 1.00 Å at the SER-CAT beamline ID-22 (Advanced Photon Source, Argonne National Laboratory).

X-ray data collection, structure solution and model building

Diffraction data were processed with the HKL2000 suite (*49*). The ternary complex crystal diffraction data were corrected for anisotropy by http://services.mbi.ucla.edu/anisoscale/ with truncations to 4.3 Å, 5.0 Å, 5.0 Å along a, b, and c axes, respectively. Structure solution was obtained by molecular replacement with Phaser using structures of a Fab (PDB ID: 4JPI, for VRC34.01 Fab), or Env and PGT122 in (PDB ID: 4TVP) (*44*), and VRC34.01 Fab (for ternary complex and fusion peptide/VRC34.01 Fab complex) as search models. Refinement was carried out with Phenix (*50*). Model building was carried out with Coot (*51*). The Ramachandran plot as determined by MOLPROBITY (*52*) showed 96% (VRC34.01 Fab), 90% (ternary complex) and 95% (fusion peptide/VRC34.01 Fab complex) of all residues in favored regions. Data collection and refinement statistics are shown in table S1.

Surface plasmon resonance assay

Affinities and kinetics of antibody binding to SOSIP and DS-SOSIP were assessed by surface plasmon resonance on a Biacore T-200 (GE Healthcare) at 20 °C with buffer HBS-EP+ (10 mM HEPES, pH 7.4, 150 mM NaCl, 3 mM EDTA and 0.05% surfactant P-20). Trimer was captured either onto a 2G12 or a CD4 surface obtained by capturing 2G12 IgG or CD4-Ig, respectively, on a flow cell immobilized with ~10,000 response units (RU) of mouse anti-human Fc antibody. A 200 nM solution of 2G12 IgG or CD4-Ig, and a 500 nM solution of trimer were used to create the ligand surface. Binding of trimer to antibody was measured with successive injections different concentrations of antibody Fab fragments. Blank sensorgrams were obtained by injection of the same volume of HBS-EP+ buffer in place of antibody Fab fragments. Sensorgrams of the concentration series were corrected with corresponding blank curves and fitted globally with Biacore T200 evaluation software using a 1:1 Langmuir model of binding.

Time-course of CD4 activation of the trimers was measured at 15 °C in HBS-EP+ buffer. 17b IgG and 2G12 IgG were captured on separate flow cells of a CM5 chip immobilized with ~10,000 RU of mouse anti-human Fc antibody, by injecting a 200 nM solution of each antibody on the sensor chip surfaces at a flow rate 5 µl/min for 2 min. One flow cell immobilized with ~10,000 RU of mouse anti-human Fc antibody was used as reference flow cell. A 40 nM solution of SOSIP, either alone or in presence of 4-fold molar excess of antibody Fab fragment, were incubated in four-fold molar excess of sCD4, and samples were injected at different time points. Blank sensorgrams were obtained by injection of the same volume of HBS-EP+ buffer in place of trimer and were subtracted from reference-subtracted sensorgrams obtained with trimer samples. Binding levels in double-referenced sensorgrams were measured 40 s after sample injection.

Affinity of VRC34.01 Fab to the His-tagged fusion peptide was measured on a Ni-NTA sensor chip (GE Healthcare). 1 mM of Ni_2SO4 in running buffer (HBS-EP+) was injected for one minute (5 µl/min) to prepare the sensor surface. Fusion peptide with His-tag (100 µg/ml) was captured at 10 µl/min flow rate for 10 seconds over the nickel activated sensor surface. Interaction analysis was performed by flowing serial concentrations of antibody VRC34.01 Fab over the peptide captured sensor chip for one minute (20 µl/min). 350 mM EDTA and 3M of $MgCl_2$ were used as regeneration buffer. The data were processed with SCRUBBER-2 and double referenced by subtraction of the blank surface and a blank injection (no analyte). Binding curves were globally fitted to a 1:1 binding model.

EM data collection and processing

BG505 SOSIP.664 gp140 trimers were expressed in HEK293F cells and purified by 2G12-affinity and gel filtration chromatography as described elsewhere (*10*). VRC34.01 IgG was treated with papain to generate Fab. The resulting Fab reaction mixture was passed over Protein A affinity and gel filtration chromatography columns to remove undigested IgG, Fc domains, and papain. Trimers were incubated with a 6 molar excess of Fab overnight at room temperature and the complexes were diluted to ~0.03 mg/mL prior to application onto a carbon-coated 400 Cu mesh grid that had been glow discharged at 20 mA for 30 s. The grids were stained with 2% (w/v) uranyl formate for 45 seconds. Samples were imaged on an FEI Talos electron microscope operating at 200 keV, with an electron dose of ~ 25 $e^-/Å^2$ and a magnification of 92,000x that resulted in a pixel size of 1.57 Å at the specimen plane. Images were acquired with Leginon (*53*). Using an FEI Ceta 16M camera and a nominal defocus range of 1000-1500 nm. Stage tilts of 0, 10, 20, 30, 40, and 50° were performed to increase the amount of unique views to aid with 3D reconstruction.

Automated particle picking, stack creation, and initial 2D classification was performed in the Appion software suite (*54*). Noise and junk particles were discarded and representative class averages with unique views were used to generate an initial common-lines model using EMAN2 (*55*) followed by refinement against all 9,261 particles in Sparx (*56*). The resolution of the final reconstruction is ~17 Å based on a Fourier shell correlation of 0.5. Two-dimensional back projections of the final 3D models were generated using EMAN (*55*).

Docking of the VRC34.01-BG505 SOSIP complex into EM density map of the HIV-1 Env trimers in membrane-bound context

To analyze relative distance of fusion peptide to the HIV-1 viral membrane, the negative stain EM map of the VRC34.01-BG505 SOSIP.664 complex was first superposed with the EM density of HIV-1 Env trimers reconstructed from their membrane-bound context (EMDB 5019 and 5022, or EMDB 5457) (*28*) with program Chimera (*57*). The coordinates of VRC34.01-BG505 SOSIP.664 complex as extracted from the ternary complex crystal structure was then fitted into the EM map of the VRC34.01-BG505 SOSIP.664 complex.

Molecular Dynamics of Mannose-9 model

Using the BG505.SOSIP.664 Env trimer structure (PDB ID: 4TVP) as starting template, we modeled in a fully extended Mannose 9 moiety at each N-linked glycosylation sequon using our in-house software ***glycosylator***. The fusion peptide structure was then grafted onto our full Mannose 9 model and solvated in a 181 x 177 x 177 $Å^3$ water box. The system was neutralized by the addition of NaCl at a concentration of 150 mM. The CHARMM36 force field was used for the parameterization of the protein (including CMAP corrections) (*58*) and the mannose 9 (*59*). TIP3P parameterization (*60*) was used to describe the water molecules.

The molecular simulation was carried out using ACEMD (*29*) molecular dynamics software on their METROCUBO workstation (https://www.acellera.com/products/GPU-hardware-molecular-dynamics-metrocubo/). The system was minimized for 2000 steps, followed by equilibration using the NPT ensemble for 50 ns at 1 atm and 300 K using a time-step of 2 fs. We also used rigid bonds and cutoff of 9 Å using PME for long range electrostatics. During the equilibration phase, heavy atoms on the protein were constrained by a 1 kcal/mol·$Å^2$ spring constant and slowly relaxed over the first 5 ns. Following the relaxation phase, the protein was allowed to move freely and simulated for 500 ns under the NVT ensemble using ACEMD's NVT ensemble with a Langevin thermostat. To achieve a time-step of 4 ps, we used damping at a frequency of 0.1 ps^{-1} along with a hydrogen mass repartitioning scheme.

In order to determine the distance from each residue of the fusion peptide to the membrane, we first created a POPC membrane bilayer disk with a radius of 95 Å using the VMD membrane plug-in (http://www.ks.uiuc.edu/Research/vmd/plugins/membrane/). Colores (*61*) was then used to separately dock the membrane and Env trimer into a cryo-electron tomography map (EMDB 5457). The distance to the membrane was defined as the distance between the closest phosphate head group and each geometric center of the side chain for each residue in the fusion peptide.

All solvent-accessible surface area (SASA) calculations were carried out using the program NSC (*62*). Fully extended conformations Gly-Xxx-Gly tripeptide conformations for all amino acids were used to normalize the solvent-accessible surface areas.

smFRET data acquisition and analysis

HIV-1 JR-FL virions carrying a single dually-tagged Env molecule were produced and enzymatically labeled with donor Cy3B (3S) and acceptor Cy5 (4S) COT* fluorophores in the V1 and V4 loops of gp120, respectively. Fluorescently labeled virions were immobilized on streptavidin-coated quartz microscope slides and imaged on a prism-based total internal reflection fluorescence microscope. Movies were recorded at 25 frames/s for 40 s. smFRET imaging was performed in buffer containing 50 mM Tris pH 7.4, 50 mM NaCl, and a cocktail of triplet-state quenchers. 2 mM protocatechuic acid (PCA) and 8 nM protocatechuic 3,4-dioxygenase (PCD) were also included to remove molecular oxygen. Where indicated, surface-bound viruses were incubated with 0.1 mg/ml VRC34.01 antibody for 30 minutes at room temperature before imaging. Data analysis was performed using custom Matlab software. Fluorescence trajectories were extracted from the movies, and used to calculate FRET efficiency where FRET = IA/(ID+IA). FRET trajectories were compiled into histograms and fit to the sum of three Gaussian distributions. Error bars were generated by propagating the uncertainties of the fits through the occupancy calculation.

VRC34-epitope scaffold design

VRC34-epitope scaffold constructs were designed by adding fusion peptide (residues 512-519) to the N-terminus of various scaffold proteins (fig. S19). An N-linked glycosylation site was also introduced to some of the constructs to resemble glycan N88 on HIV-1 Env protein. The VRC34-epitope scaffold (FP-1M6T-K42N) used for human sera mapping in this study was designed by connecting the BG505 fusion peptide (512-519) to the N-terminus of a four helix bundle (*63*) using a "GGG" linker, with a N-linked glycosylation sequon introduced at residue 42 of the scaffold (K42N). A control scaffold (1M6T-K42N) with the glycan introduced but with out the fusion peptide (512-519) was also used.

Screening of fusion peptide-based immunogen design constructs

High throughput ELISA analysis was performed to select the best VRC34-epitope scaffolds based on the combination of their expression level and affinity to VRC34.01 mAb. In detail, a 96-well microplate-formatted transient gene expression approach was used to achieve high-throughput expression of various design constructs as described previously (*64*). Briefly, 24 hours prior to DNA-transient transfection, 100 µl per well of physiologically growing HEK 293T cells were seeded into a 96-well microplate at a density of $2.5x10^5$ cells/ml in expression medium (Dulbecco's Modified Eagle Medium and GlutaMAX, supplemented with 6% Fetal Bovine Serum and 1x-Non-Essential Amino Acids) (Invitrogen, CA), and incubated at 37°C, 5% CO_2. Two hours prior to transfection, 100 µl per well of spent medium was replaced with 60 µl of fresh expression medium. For transient transfection, DNA-TrueFect-Max complex per well was prepared by mixing 0.25 µg plasmid DNA in 10 µl of Opti-MEM transfection medium (Invitrogen, CA) with 0.75 µl of TrueFect-Max (United BioSystems, VA) in 10 µl of Opti-MEM, and incubating for 15 min, and then mixed with growing cells in the 96-well plate and incubated at 37°C, 5% CO_2. One day post transfection, 25 µl per well of enriched medium, ProBooster Protein Expression Enhancer for Adherent cell (ABI, VA) was fed. On day three and four post transfection, 96-well culture plate was exposed to oxygen in the sterilized air hood once per day. Five days after transfection, the antigenicity of

immunogens was characterized by ELISA assay. Briefly, 30 µl per well of supernatant expressed in the 96-well microplate was diluted with 70 µl of PBS in a Nickel coated 96-well ELISA plate (Thermo, IL) and incubated for two hours at room temperature (RT). After washing with PBS + 0.05% Tween 20, 100 ul per well of primary antibody at a concentration of 10 ug/ml in PBS with 0.5 % (W/V) dry milk and 0.02% tween 20 was incubated for 1 hour at RT. After washing, 100 ul per well of Horseradish peroxidase (HRP)-conjugated goat anti-human IgG antibody (Jackson ImmunoResearch Laboratories Inc., PA) at 1:10,000 in PBS with 1.0 % (W/V) dry milk and 0.02% tween 20 was incubated for 30 min at RT. After washing, the reaction signal was developed using BioFX-TMB (SurModics, MN) at RT for 10 min, and then stopped with 1 N H_2SO_4. The readout was measured at a wavelength of 450 nm. Constructs with highest readout were selected.

Author contributions

RK, isolated and characterized N123-VRC34 lineage, co-determined mechanism of neutralization, mapped fusion peptide-directed antibodies in human sera and wrote the paper; KX, co-determined structures of Fab VRC34.01 alone, with peptide, and in complex with HIV-1 Env trimer and wrote paper; TZ, co-determined structures of VRC34.01 alone and in complex with HIV-1 Env trimer and wrote paper, PA, co-determined mechanism of VRC34.01 neutralization and wrote paper; TML and CS, performed and analyzed molecular dynamics simulation of fully glycosylated HIV-1 Env trimer; GO, determined negative stain EM structures; KL, co-determined structure of Fab VRC34.01 with fusion peptide; JDT, co-isolated and characterized VRC34.01; RTB, MKL and KM, performed high throughput neutralization; EMC, NDR and MP, contributed to antigen-specific cell sorting; CWC, contributed to sera mapping; LC, performed peptide affinity analysis; GC, MGJ and YY, contributed to the VRC34-epitope scaffold design; SD, contributed BG505 mutant viruses; AD, contributed protein production; JG contributed to mechanistic analysis; XM, SB, WM performed smFRET analysis; ISG, performed HIV fusion peptide and fingerprint analysis; MGJ, determined HA fusion peptide analysis; DRB and WCK, contributed antibody PGT122; MC and JH, contributed donor N123 samples; ABW, headed EM structure determination; PDK, headed structure determination and wrote paper; JRM, headed antibody identification and characterization and wrote the paper.

A

Clade	Virus	N123 serum
A	KER2018.11	458
	RW020.2	241
	Q168.a2	222
	Q23.17	339
	Q769.h5	660
	BG505	161
B	6101.1	59
	BaL.01	731
	BG1168.01	148
	CAAN.A2	112
	JRCSF.JB	558
	JR-FL.JB	523
	PVO.04	1160
	THRO.18	130
	TRJO.58	31
	TRO.11	544
	YU2.DG	158
C	ZA012.29	79
	DU156.12	611
	DU422.01	252
	ZM106.9	211
	ZM55.28a	153
MuLV (control)		17
No. of viruses		22
Neutralized (ID50<1:100)		19
% virus neutralized		86%
Geometric mean ID50		209

B

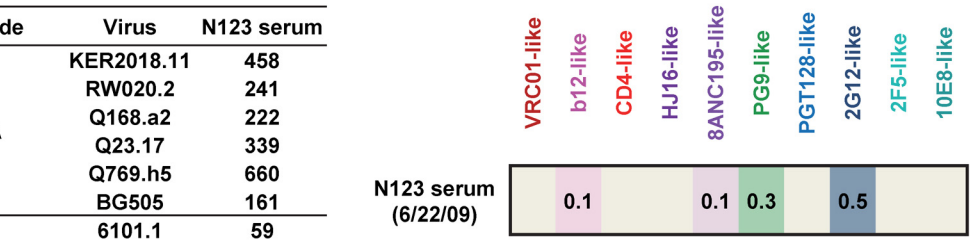

C

BG505	N123 serum		PG9	
	ID50	fold change	IC50 (μg/ml)	fold change
wildtype	161		0.029	
N160K	122	1.3	>50	>1724
K169E	135	1.2	>50	>1724

JRCSF	N123 serum		2G12	
	ID50	fold change	IC50 (μg/ml)	fold change
wildtype	309		0.229	
N295A	209	1.5	>50	>218
N332A	256	1.2	>50	>218
N339A	384	0.8	6.29	27.5
N386A	473	0.7	11.5	50.2
N392A	198	1.6	>50	>218

Fig. S1. Neutralization titers and serologic mapping of donor N123 serum.
(A) Neutralization titers of N123 serum on a panel of 22 HIV-1 Env-pseudotyped viruses. The serum dilutions corresponding to a 50% inhibition (ID_{50}) of virus entry into TZM-bl cells are shown. An ID_{50} greater than 1:100 is considered as positive neutralization. Geometric mean ID_{50} were calculated based on viruses with ID_{50} that is greater than 1:100. (B) Serological fingerprint of the N123 serum (*32, 44*). The score shows the estimated contribution of each type from a reference set of antibodies, with a score of 1 indicating 100% contribution. These scores, however, are only useful for sera for which the dominant specificities are found in the reference set. (C) N123 serum neutralization against wildtype and mutant viruses. The ID_{50} and ID_{50} fold change are shown. A mutant with ID_{50} fold change that is greater than 3 is considered to be critical for serum/antibody neutralization. N123 serum neutralization is not sensitive to PG9-specific and 2G12-specific mutations.

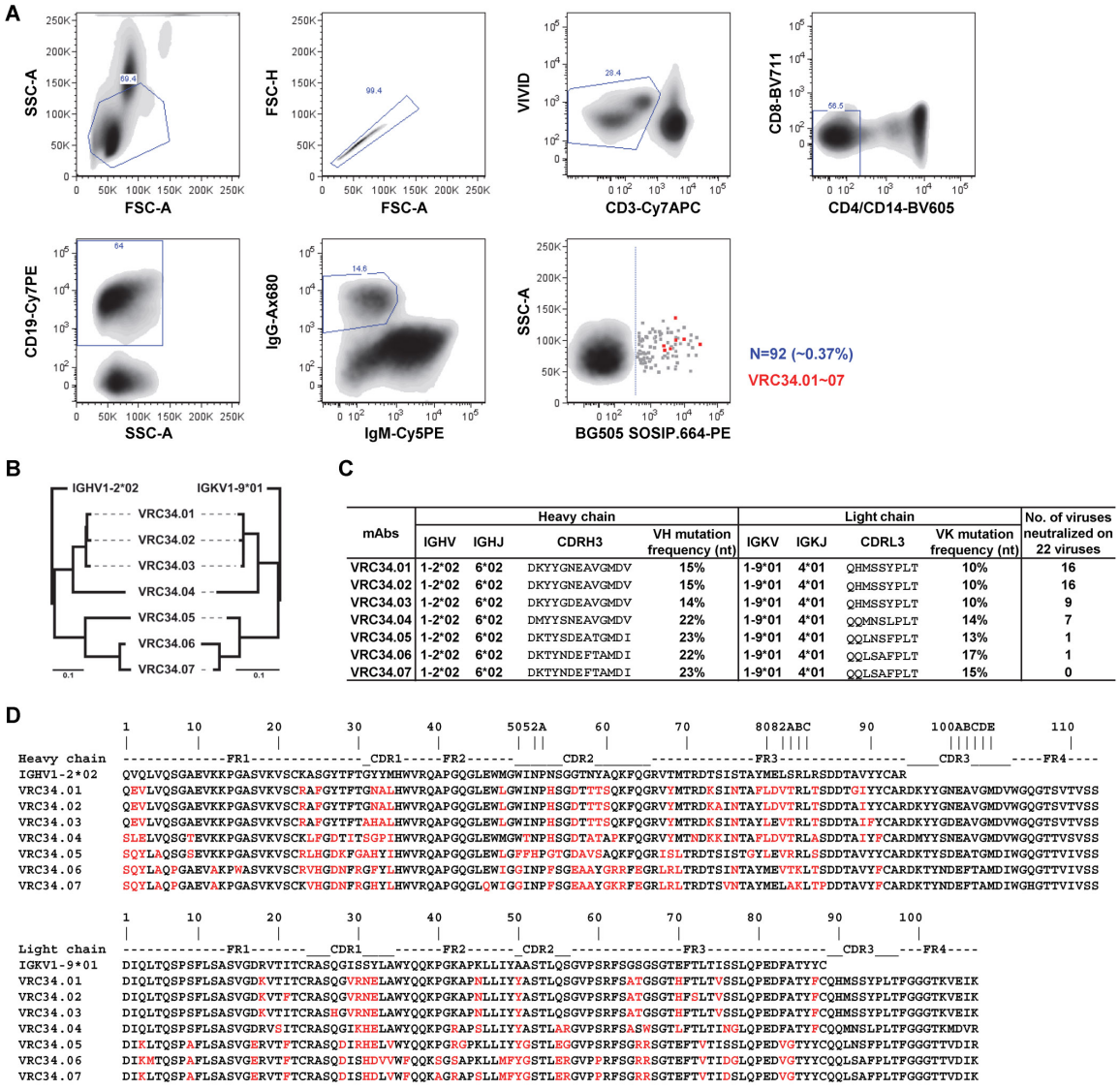

mAbs	Heavy chain				Light chain				No. of viruses neutralized on 22 viruses
	IGHV	IGHJ	CDRH3	VH mutation frequency (nt)	IGKV	IGKJ	CDRL3	VK mutation frequency (nt)	
VRC34.01	1-2*02	6*02	DKYYGNEAVGMDV	15%	1-9*01	4*01	QHMSSYPLT	10%	16
VRC34.02	1-2*02	6*02	DKYYGNEAVGMDV	15%	1-9*01	4*01	QHMSSYPLT	10%	16
VRC34.03	1-2*02	6*02	DKYYGDEAVGMDV	14%	1-9*01	4*01	QHMSSYPLT	10%	9
VRC34.04	1-2*02	6*02	DMYYSNEAVGMDV	22%	1-9*01	4*01	QQMNSLPLT	14%	7
VRC34.05	1-2*02	6*02	DKTYSDEATGMDI	23%	1-9*01	4*01	QQLNSFPLT	13%	1
VRC34.06	1-2*02	6*02	DKTYNDEFTAMDI	22%	1-9*01	4*01	QQLSAFPLT	17%	1
VRC34.07	1-2*02	6*02	DKTYNDEFTAMDI	23%	1-9*01	4*01	QQLSAFPLT	15%	0

```
Heavy chain  ------------FR1--------------CDR1-----FR2------______CDR2_______------------FR3-----------------____CDR3_____----FR4----
IGHV1-2*02   QVQLVQSGAEVKKPGASVKVSCKASGYTFTGYYMHWVRQAPGQGLEWMGWINPNSGGTNYAQKFQGRVTMTRDTSISTAYMELSRLRSDDTAVYYCAR
VRC34.01     QEVLVQSGAEVKKPGASVKVSCRAFGYTFTGNALHWVRQAPGQGLEWLGWINPHSGDTTTSQKFQGRVYMTRDKSINTAFLDVTRLTSDDTGIYYCARDKYYGNEAVGMDVWGQGTSVTVSS
VRC34.02     QEVLVQSGAEVKKPGASVKVSCRAFGYTFTGNALHWVRQAPGQGLEWLGWINPHSGDTTTSQKFQGRVYMTRDKAINTAYLDVTRLTSDDTAIYYCARDKYYGNEAVGMDVWGQGTSVTVSS
VRC34.03     QEVLVQSGAEVKKPGASVKVSCRAFGYTFTAHALHWVRQAPGQGLEWLGWINPHSGDTTTSQKFQGRVYMTRDKSINTAYLEVTRLTSDDTAIFYCARDKYYGDEAVGMDVWGQGTSVTVSS
VRC34.04     SLELVQSGTEVKKPGASVKVSCKLFGDTITSGPIHWVRQAPGQGLEWMGWTNPHSGDTATAPKFQGRVYMTNDKKINTAFLDVTRLASDDTAIYFCARDMYYSNEAVGMDVWGQGTTVSVSS
VRC34.05     SQYLAQSGSEVKKPGASVKVSCRLHGDKFGAHYIHWVRQAPGQGLEWLGFFHPGTGDAVSAQKFQGRISLTRDTSISTGYLEVRRLSSDDTAVYYCARDKTYSDEATGMDIWGQGTTVIVSS
VRC34.06     SQYLAQPGAEVAKPWASVKVSCRVHGDNFRGFYLHWVRQAPGQGLEWIGGINPFSGEAAYGRRFEGRLRLTRDTSINTAYMEVTKLTSDDTAVYFCARDKTYNDEFTAMDIWGQGTTVIVSS
VRC34.07     SQYLAQPGAEVAKPGASVKVSCKVHGDNFRGHYLHWVRQAPGQGLQWIGGINPFSGEAAYGKRFEGRLRLTRDTSVNTAYMELAKLTPDDTAVYFCARDKTYNDEFTAMDIWGHGTTVIVSS

Light chain  ------------FR1-------___CDR1___------FR2-------CDR2__--------------FR3---------------__CDR3___---FR4----
IGKV1-9*01   DIQLTQSPSFLSASVGDRVTITCRASQGISSYLAWYQQKPGKAPKLLIYAASTLQSGVPSRFSGSGSGTEFTLTISSLQPEDFATYYC
VRC34.01     DIQLTQSPSFLSASVGDKVTITCRASQGVRNELAWYQQKPGKAPNLLIYYASTLQSGVPSRFSATGSGTHFTLTVSSLQPEDFATYFCQHMSSYPLTFGGGTKVEIK
VRC34.02     DIQLTQSPSFLSASVGDKVTFTCRASQGVRNELAWYQQKPGKAPNLLIYYASTLQSGVPSRFSATGSGTHFSLTVSSLQPEDFATYFCQHMSSYPLTFGGGTKVEIK
VRC34.03     DIQLTQSPSFLSASVGDKVTITCRASHGVRNELAWYQQKPGKAPNLLIYYASTLQSGVPSRFSATGSGTHFTLTVSSLQPEDFATYFCQHMSSYPLTFGGGTKVEIK
VRC34.04     DIQLTQSPSFLSASVGDRVSITCRASQGIKHELAWYQQKPGRAPSLLIYYASTLARGVPSRFSASWSGTLFTLTINGLQPEDFATYFCQQMNSLPLTFGGGTKMDVR
VRC34.05     DIKLTQSPAFLSASVGERVTFTCRASQDIRHELVWYQQKPGRGPKLLIYYGSTLEGGVPSRFSGRRSGTEFTVTISSLQPEDVGTYYCQQLNSFPLTFGGGTTVDIR
VRC34.06     DIKMTQSPAFLSASVGERVTFTCRASQDISHDVVWFQQKSGSAPKLLMFYGSTLERGVPPRFSGRRSGTEFTVTIDGLQPEDVGTYYCQQLSAFPLTFGGGTTVDIK
VRC34.07     DIKLTQSPAFLSASVGERVTFTCRASQDISHDLVWFQQKAGRAPSLLMFYGSTLERGVPPRFSGRRSGTEFTVTIDSLQPEDVGTYYCQQLSAFPLTFGGGTTVDIK
```

Fig. S2. Isolation and genetic characterization of VRC34 lineage mAbs. (A) Antigen-specific sorting of PBMCs from donor N123 (6/22/09). 40 million PBMCs were stained for sorting. The gating strategy for live memory B cells (VIVID-/CD3-/CD4-/CD8-/CD14-/CD19+/IgG+/IgM-) is shown. The cells are shown using a density plot format and the fluorescence intensity of the staining is shown. A total of 92 B cells (~0.37% of IgG+/IgM- B cells) that were positively stained with probe BG505 SOSIP.664-PE were sorted into 96-well plates containing lysis buffer. The blue line indicates gating cutoff. VRC34.01-07 B cells are highlighted in red. FSC-A, forward scatter area; FSC-H, forward scatter height; and SSC, side scatter area. (B) Maximum likelihood tree of nucleotide sequences of VRC34.01-07 heavy and light chain variable (V) region. (C) Genetic characteristics for VRC34 lineage mAbs. Gene assignment and mutation frequency were determined using the IMGT database (http://imgt.org). The CDR3 sequences were determined according to the Kabat definition. (D) Amino acid sequence alignment of heavy and light chain variable regions. Antibody residue numbering, framework regions (FR) and complementarity-determining regions are based on Kabat nomenclature.

IC50 (μg/mL)		VRC01	N123-VRC34 lineage mAbs							N123 serum
			VRC34.01	VRC34.02	VRC34.03	VRC34.04	VRC34.05	VRC34.06	VRC34.07	
A	KER2018.11	0.3700	0.0940	0.0940	0.5600	0.5450	>50	>50	>50	458
	RW020.2	0.1850	0.8910	0.7910	>50	2.0000	>50	>50	>50	241
	Q168.a2	0.0930	0.0750	0.1020	0.2950	0.2540	>50	>50	>50	222
	Q23.17	0.0770	0.0520	0.0620	0.2350	0.2810	>50	>50	>50	339
	Q769.h5	0.0620	>50	>50	>50	>50	>50	>50	>50	660
	BG505	0.0520	0.1310	0.1000	0.7070	0.1120	>50	>50	>50	161
B	6101.1	0.0750	0.4970	0.5950	1.5200	>50	>50	>50	>50	59
	BaL.01	0.0590	0.1100	0.1440	0.3100	0.0710	>50	>50	>50	731
	BG1168.01	0.6570	0.3300	0.4670	>50	>50	0.9190	>50	>50	148
	CAAN.A2	0.9300	0.3190	0.4410	8.5400	>50	>50	>50	>50	112
	JRCSF.JB	0.1630	0.3090	0.5630	>50	>50	>50	>50	>50	558
	JR-FL.JB	0.0390	0.1360	0.1220	0.3130	>50	>50	>50	>50	523
	PVO.04	0.3870	>50	>50	>50	>50	>50	>50	>50	1160
	THRO.18	5.6000	>50	>50	>50	>50	>50	>50	>50	130
	TRJO.58	0.0840	7.8300	5.5400	>50	>50	>50	>50	>50	31
	TRO.11	0.3660	>50	>50	>50	>50	>50	>50	>50	544
	YU2.DG	0.1010	2.0100	2.7900	>50	>50	>50	>50	>50	158
C	ZA012.29	0.2480	0.9880	1.0300	>50	>50	>50	>50	>50	79
	DU156.12	0.0930	>50	>50	>50	1.0400	>50	0.4040	>50	611
	DU422.01	>50	1.9400	2.2400	>50	>50	>50	>50	>50	252
	ZM106.9	0.2960	>50	>50	>50	>50	>50	>50	>50	211
	ZM55.28a	0.3450	0.2540	0.4680	19.0000	>50	>50	>50	>50	153
No. of viruses		22	22	22	22	22	22	22	22	21
Neutralized (IC50<50)		21	16	16	9	7	1	1	0	18
% virus neutralized		95	73	73	41	32	5	5	0	86
Geometric mean IC50		0.1855	0.3599	0.4204	0.9544	0.3500	0.9190	0.4040	N/A	248

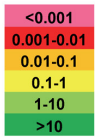

Fig. S3. Neutralization titers (IC_{50}) of VRC34 lineage mAbs on 22 HIV-1 Env-pseudotyped viruses. Geometric mean IC_{50} were calculated based on viruses with IC_{50} that is lower than 50 μg/ml.

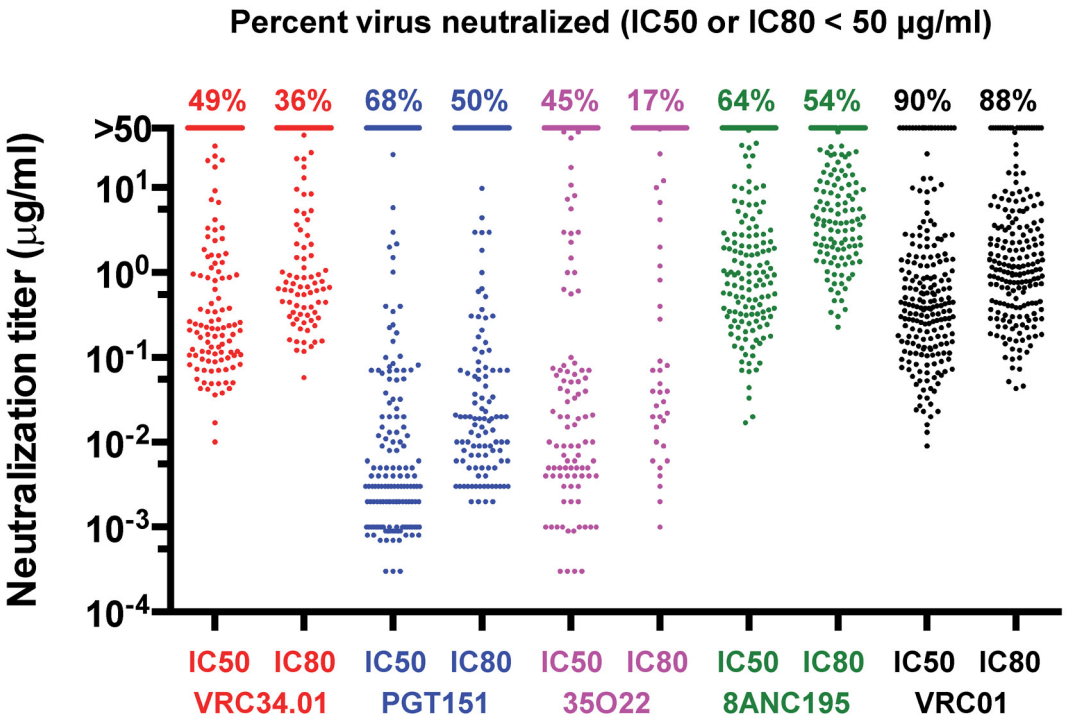

Fig. S4. VRC34.01 neutralization on a panel of 208 HIV-1 strains. The neutralization titers (IC_{50} and IC_{80}) against each virus are shown as scatter plots. Those viruses not neutralized at 50 µg/ml are shown as >50 µg/ml and the percent virus neutralized (IC_{50} or IC_{80} <50 µg/ml) are shown at the top.

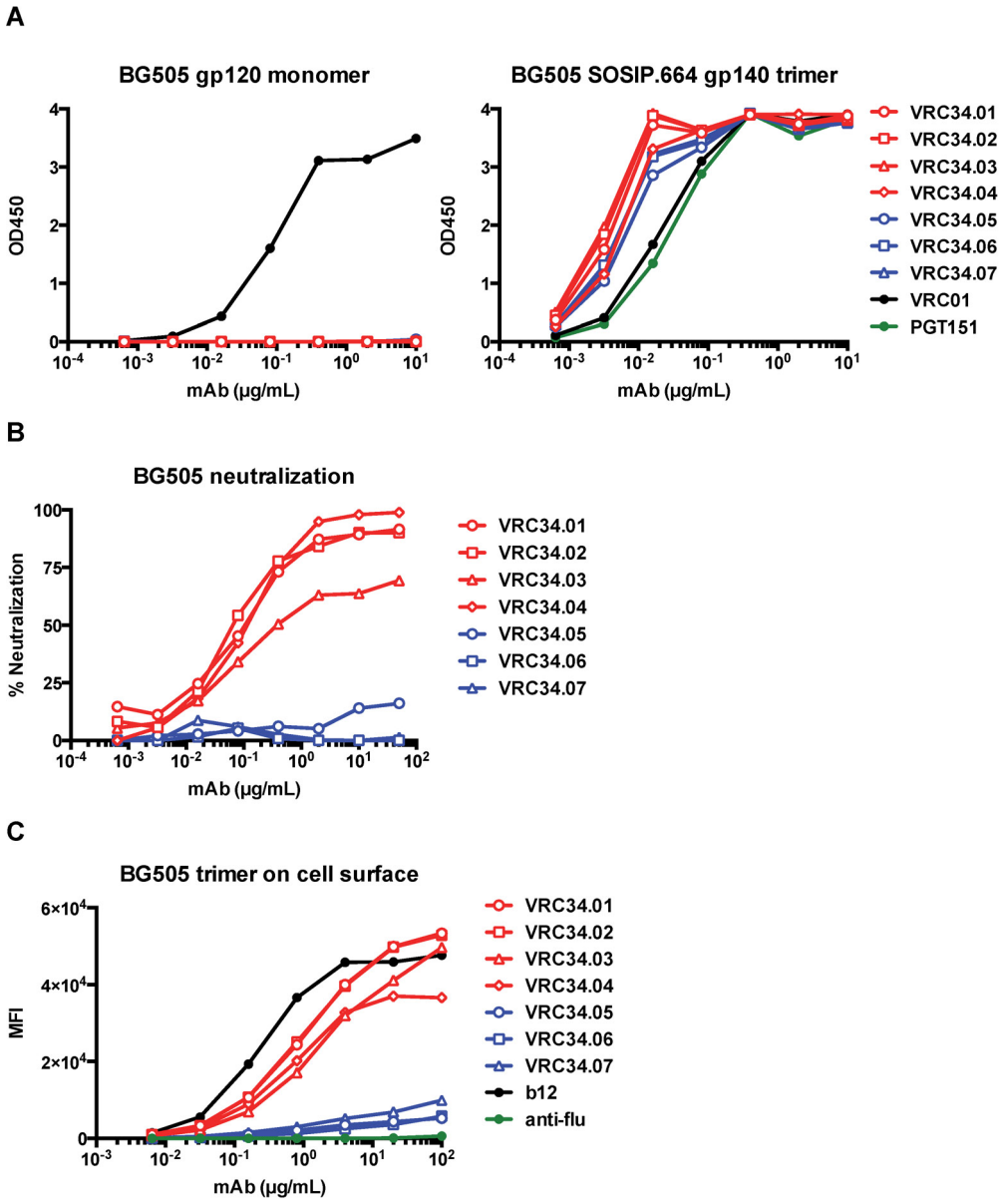

Fig. S5. Binding characteristics of VRC34 linage mAbs. (A) Binding of VRC34 lineage mAbs on BG505 gp120 monomer (left) and SOSIP.664 gp140 trimer (right) in ELISA. Broad neutralizers (VRC34.01-04) are highlighted in red and weak neutralizers (VRC34.05-07) are highlighted in blue. (B) Neutralization curves of VRC34.01-07 against the BG505 Env-pseudovirus. At each mAb concentration, the average % neutralization of duplicate wells is shown. (C) Antibody staining of 293T cells with surface expression of BG505 Env trimer. At each mAb concentration, at least 10,000 cells were assessed and the median fluorescence intensity (MFI) is shown. (A-C) Representative of two to three independent experiments is shown.

Cold competitor mAbs (10 µg/ml)		% inhibition of biotin-mAb binding			
		Biotin-mAbs			
		VRC34.01	PGT151	35O22	8ANC195
gp120-gp41 interface	VRC34.01	98%	60%	33%	6%
	PGT151	26%	60%	0%	13%
	35O22	28%	0%	58%	21%
	8ANC195	2%	44%	38%	22%
CD4bs	VRC01	2%	37%	18%	19%
V1V2-apex	PG9	8%	1%	9%	12%
	VRC26.09	5%	0%	5%	8%
	PGT145	7%	0%	7%	10%
Glycan V3	2G12	23%	33%	18%	16%
	PGT128	15%	17%	20%	20%

>80%
50-80%
<50%

Fig. S6. Competition ELISA. BG505 SOSIP.664 trimer protein was captured on ELISA plate by D7324 antibody. 10 µg/ml cold competitor mAbs were added to the plates 15 minutes prior of adding biotin labeled mAbs. Percent inhibition of biotin-mAb binding was calculated by comparing cold competitor mAbs versus PBS control.

Neutralization IC_{50} fold change				
BG505 mutants	VRC34.01	PGT151	8ANC195	VRC01
Glycan mutants				
N88Q	>385	1.0	0.9	1.3
N133Q	1.5	1.5	0.9	0.7
N137Q	1.3	1.5	0.7	1.1
N156Q	0.9	1.5	1.0	1.4
N160K	0.7	0.5	0.4	0.7
N185eQ	0.9	1.0	0.8	0.8
N185hQ	1.1	1.0	0.8	1.2
N197D	0.3	0.3	0.7	0.1
N234A	1.2	1.0	>500	0.7
N262Q	0.3	0.5	0.6	0.6
T278A	1.2	1.3	>500	0.3
N295Q	1.0	1.0	0.8	1.0
N301A	0.3	1.5	0.6	0.3
T332N	0.6	0.8	0.4	0.6
N339Q	1.0	0.8	0.4	0.7
N355Q	1.5	1.3	0.4	0.5
N363Q	0.6	0.8	0.5	0.7
N386Q	0.9	0.5	0.5	0.5
N392Q	0.7	0.5	0.4	0.4
N406Q	0.6	1.0	0.8	0.9
N411Q	0.8	1.3	0.9	1.0
N611Q	0.1	8.0	0.6	1.2
N611D	0.1	44.0	0.8	1.3
N625Q	1.6	0.8	0.6	0.9
N625A	1.0	0.8	0.4	0.7
N625D	1.4	0.5	0.3	0.5
N637Q	0.8	0.5	0.6	0.5
N637K	0.4	1.3	0.8	0.4

Fig. S7. VRC34.01 neutralization against BG505 Env-pseudotyped viruses with single amino acid mutations at N-linked glycosylation sites. Antibody neutralization was tested on the wildtype BG505 Env pseudovirus and 28 glycosylation site mutants, in which 27 mutants knock out N-linked glycosylation site by substituting ASN (N) with Gln (Q), Lys (K), Asp (D) or Ala (A), or by substituting Thr (T) with Ala (A), and T332N knocks in a glycosylation site. The amino acid numbering is based on HIV-1 HxB2 sequence. The neutralization IC_{50} titer was calculated and the IC_{50} fold change caused by each mutation is shown. A value larger than 1 indicates that the mutant is more resistant while a value less than 1 indicates that the mutant is more sensitive. A >5 fold change (5 fold more resistant) is highlighted in red, while <0.2 fold change (5 fold more sensitive) is highlighted in blue. Antibody 35O22 was not tested because it does not neutralize wildtype BG505.

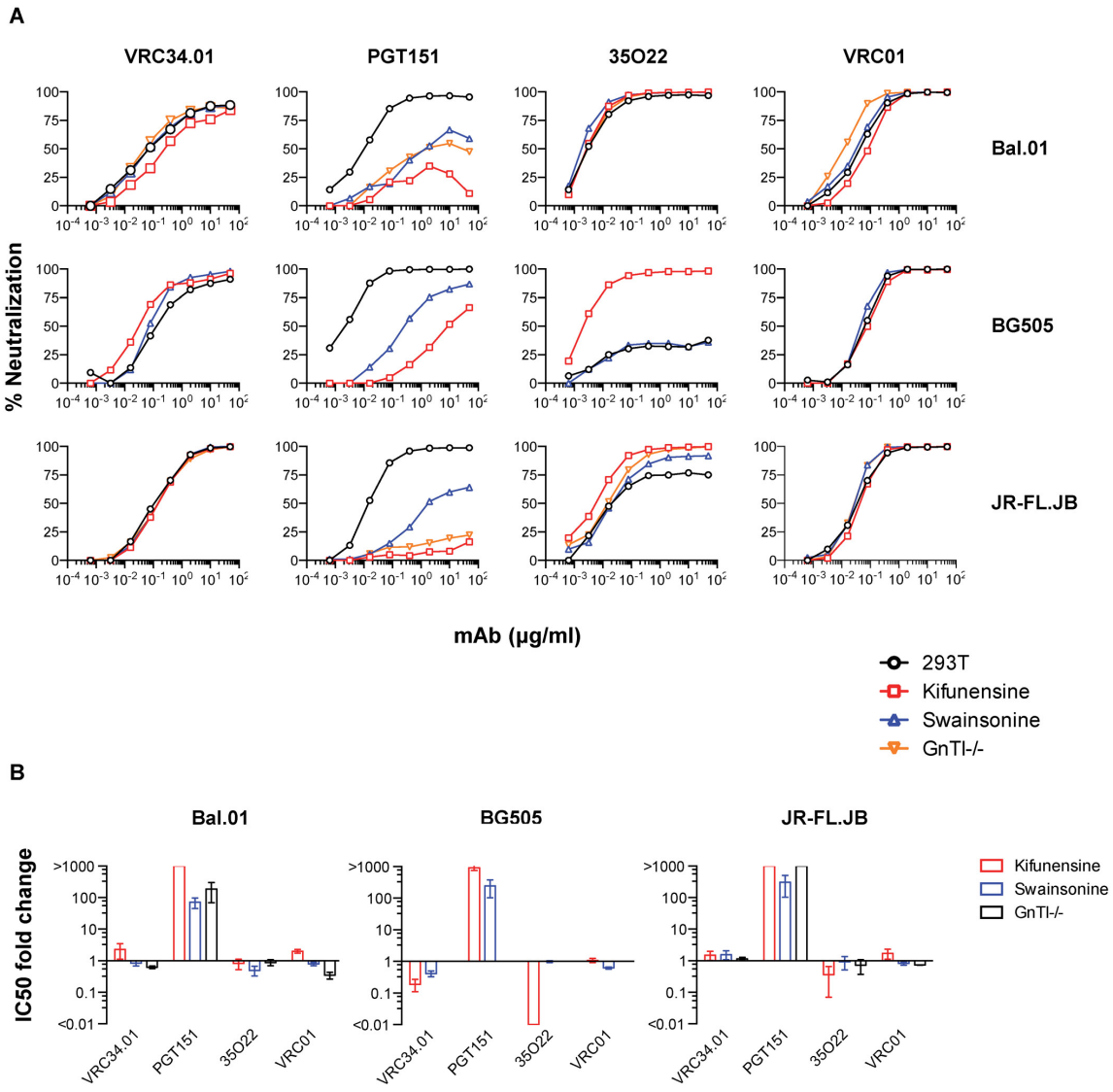

Fig. S8. mAb neutralization against viruses grown in 293T cells with or without the presence of glycosylation inhibitors kifunensine, swainsonine or in GnTI-/- 293S cells. (A) Neutralization curves of VRC34.01, PGT151, 35O22 and VRC01 against Bal.01, BG505 and JR-FL.JB. One representative of three independent experiments is shown. BG505 grown in GnTI-/- 293S cells was not tested due to low infectivity. (B) IC_{50} fold change of mAb neutralization. A value of 1 indicates no change, while >1 indicates reduced neutralizing activity and <1 indicates enhanced neutralizing activity. >1000 is shown as 1000. <0.01 is shown as 0.01. Mean and standard deviation (SD) of three independent experiments are shown.

Neutralization IC_{50} fold change				
BG505 mutants	VRC34.01	PGT151	8ANC195	VRC01
Fusion peptide mutants (512-520)				
A512W	>385	>500	0.8	2.0
V513W	>385	1.0	0.9	1.8
G514W	>385	5.5	1.0	1.4
I515A	>385	0.5	1.7	1.0
G516A	>385	1.0	0.7	1.2
A517W	7.5	1.0	0.8	1.2
V518A	0.9	0.5	0.9	0.8
V518W	>385	2.0	0.8	1.5
F519A	0.4	0.4	1.1	0.9
F519W	2.5	1.0	0.6	1.2
L520A	0.9	0.5	1.1	1.3

Fig. S9. VRC34.01 neutralization against BG505 Env pseudotyped viruses with single amino acid mutation at the N-terminus of fusion peptide (AA 512-520). Antibody neutralization was tested on the wildtype BG505 Env pseudovirus and a panel of mutants. The amino acid numbering is based on HIV-1 HxB2 sequence. The neutralization IC_{50} titer was calculated and the IC_{50} fold change caused by each mutation is shown. A value larger than 1 indicates that the mutant is more resistant while a value less than 1 indicates that the mutant is more sensitive. A >5 fold change (5 fold more resistant) is highlighted in red, while <0.2 fold change (5 fold more sensitive) is highlighted in blue. Antibody 35O22 was not tested because it does not neutralize wildtype BG505.

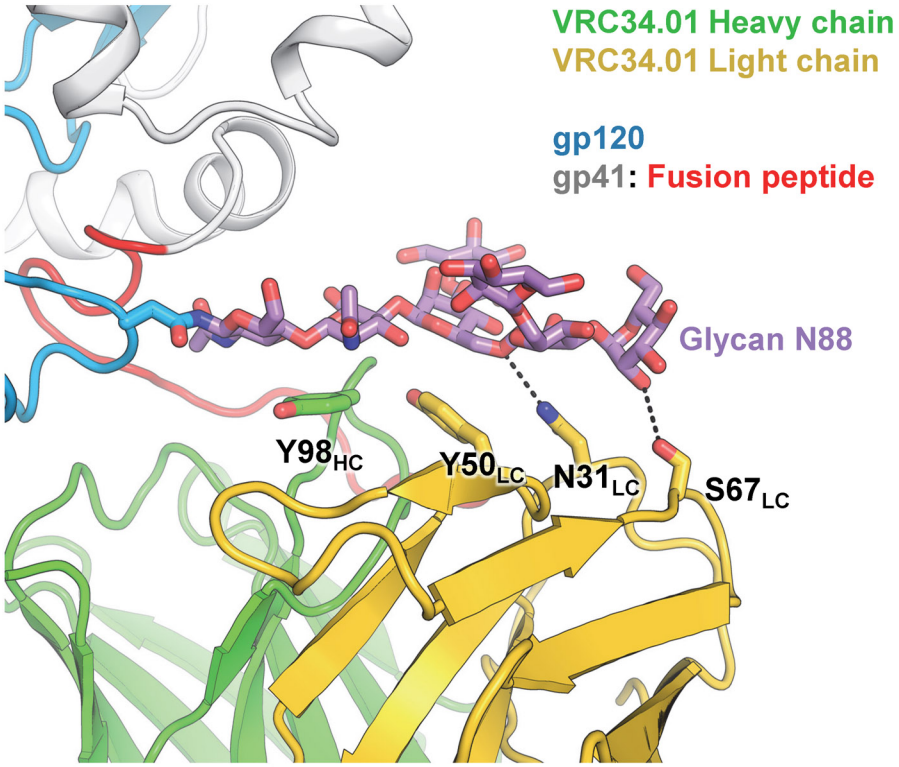

Fig. S10. VRC34.01 interaction with glycan N88 on HIV-1 gp120. Glycan N88 was targeted mostly by CDR-L1, L2 and H3 of VRC34. Y98 on CDRH3 and Y50 on CDRL2 stack their side chains with the carbohydrate backbone of glycan N88, while hydrogen-bonds formed between light chain residues N31, S67 and glycan N88 may further stabilize the interaction.

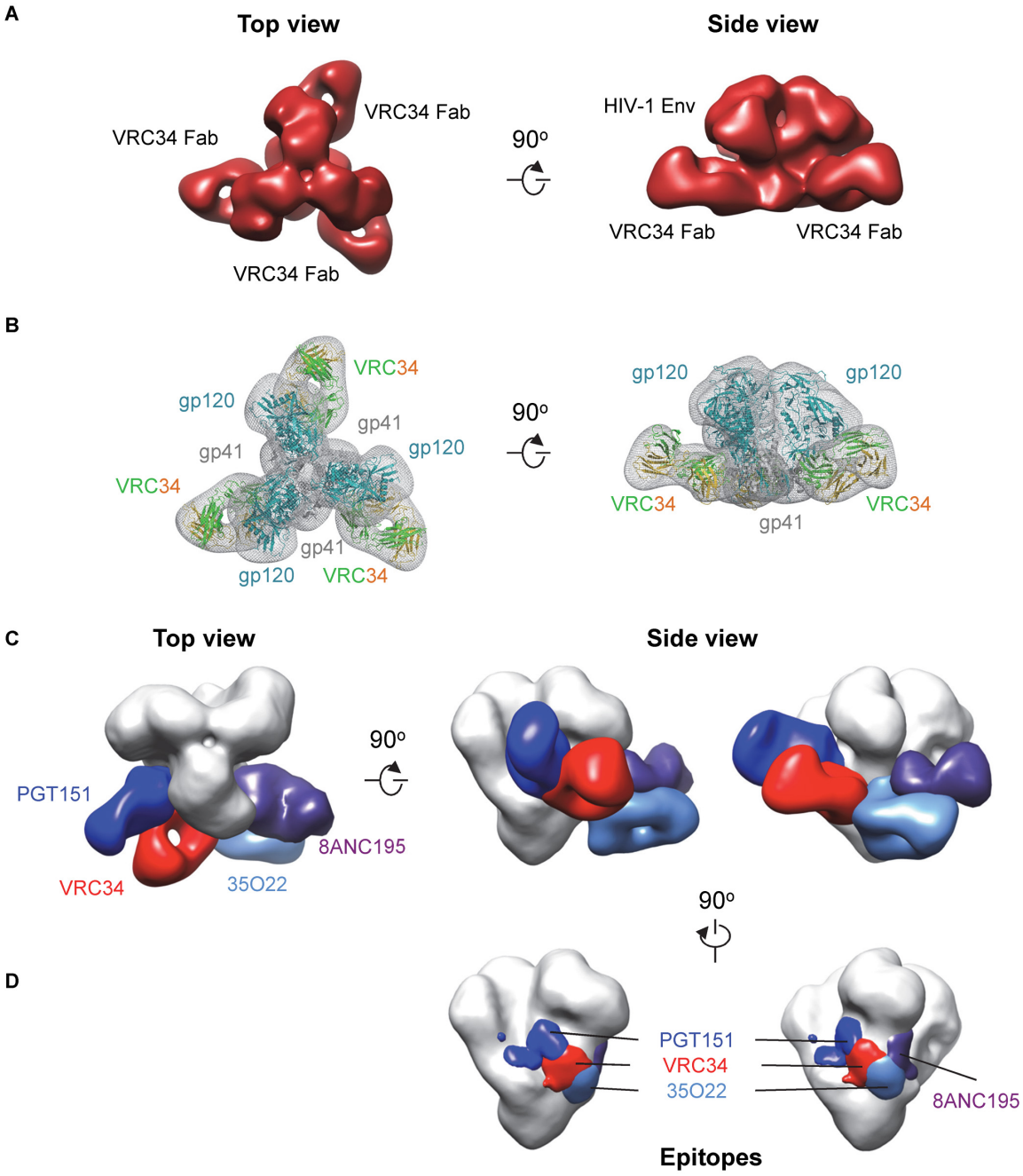

Fig. S11. Negative stain electron microscopy of VRC34.01 in complex with trimeric BG505 SOSIP. (A) ~18 Å Negative-stain EM in top and side views. (B) Negative-stain EM density with the crystal structure of BG505.SOSIP.664-VRC34 complex docked in. (C) Comparison of modes of recognition to the HIV-1 Env by antibodies PGT151, VRC34, 35O22 and 8ANC195. For clarity, antibodies were only shown to interact with one protomer. (D) Footprints of antibodies mapped onto the EM density.

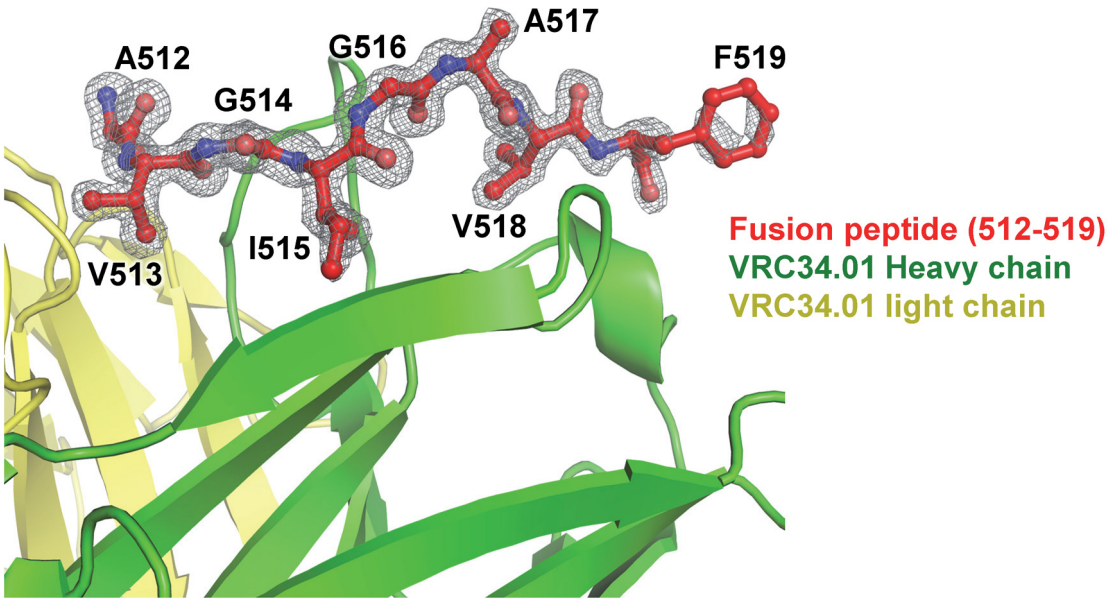

Fig. S12. Electron density map of fusion peptide in the crystal structure of VRC34.01 Fab/fusion peptide complex. Stimulated annealing omit Fo-Fc map (gray mesh) for the synthetic fusion peptide in the VRC34 Fab/peptide complex structure was contoured at 3σ. VRC34 antibody Fab was shown as ribbon, and fusion peptide residues 512-519 were shown as sticks.

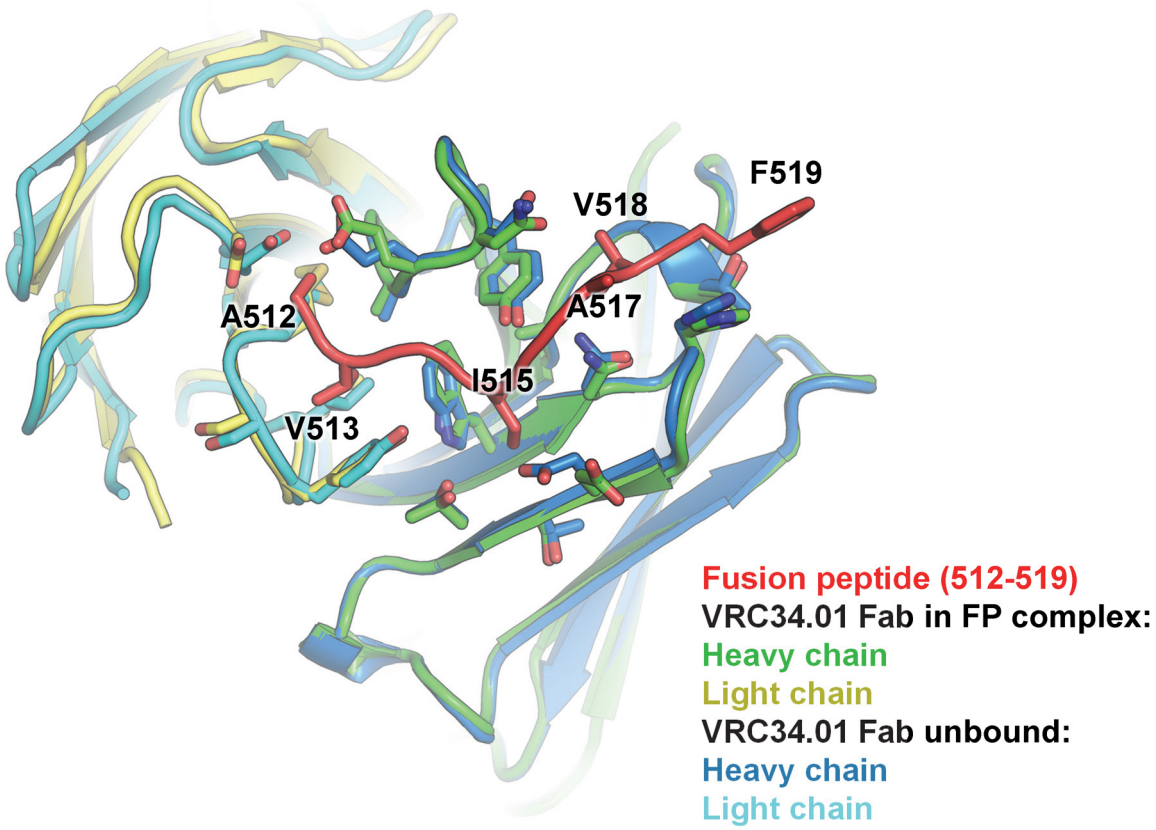

Fig. S13. Superimposition of VRC34.01 Fusion peptide contacting region between fusion peptide bound and unbound forms. With a 0.52 Å root-mean-square deviation (rmsd) over 220 VRC34.01 Fv region Cα-atoms and about 88% of the paratope residues on VRC34.01 having side-chain remaining in similar positions, there was no significant conformational change in VRC34 CDR region upon fusion peptide engagement.

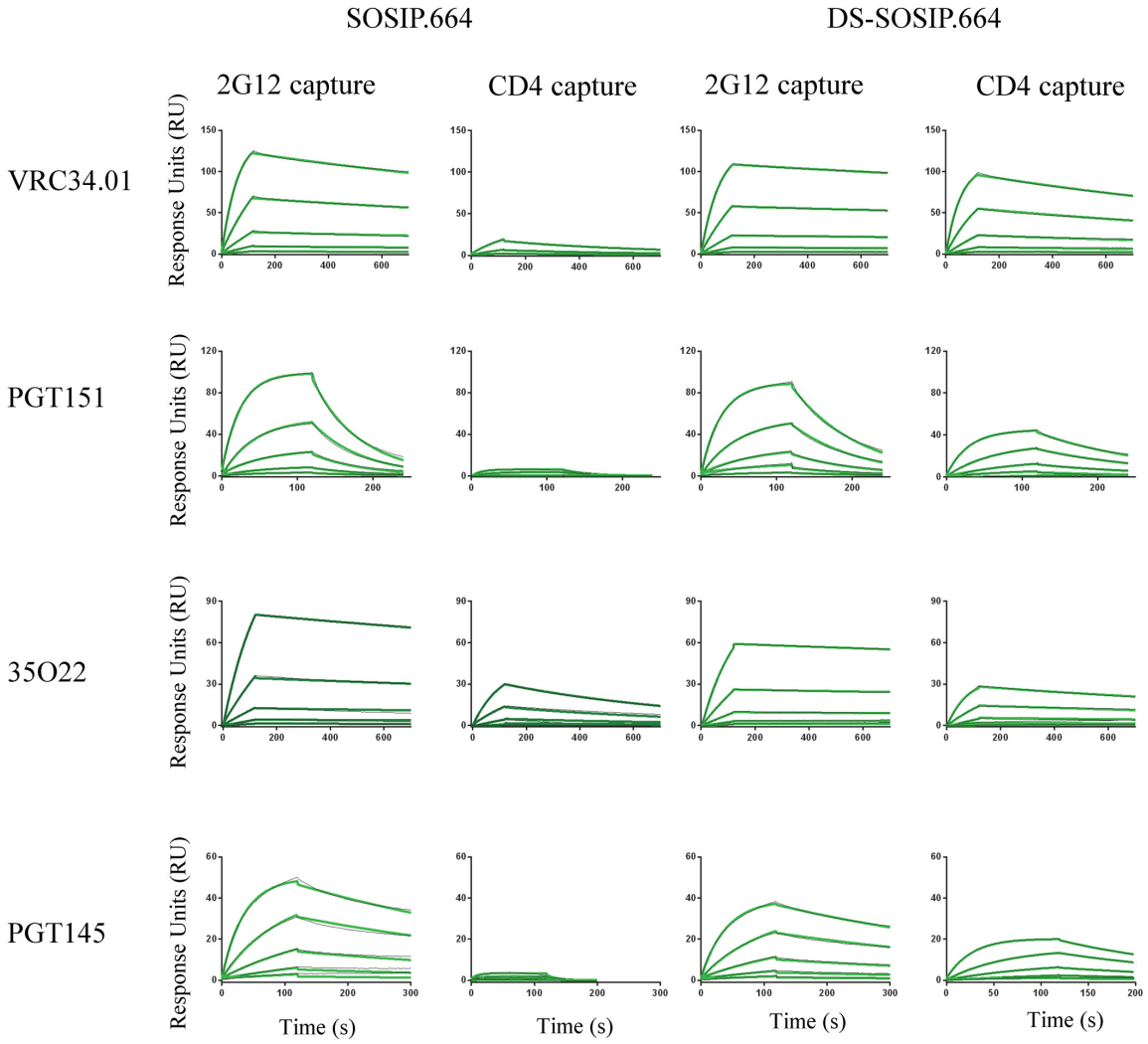

Fig. S14. Surface plasmon resonance measurement of antibody binding to SOSIP.664 and DS-SOSIP.664 trimers. Trimers were captured by either 2G12 IgG or CD4-IgG on a CM5 chip coated with human anti-Fc antibody. Antibody Fab fragments were injected at concentrations of 200, 67, 22, 7.4 and 2.5 nM concentrations. The black lines indicate blank subtracted sensorgrams and the green lines indicate global fit of each dataset to a 1:1 Langmuir binding model. Affinity and kinetics parameters are reported in Figure 3B. Representative of at least two independent experiments are shown.

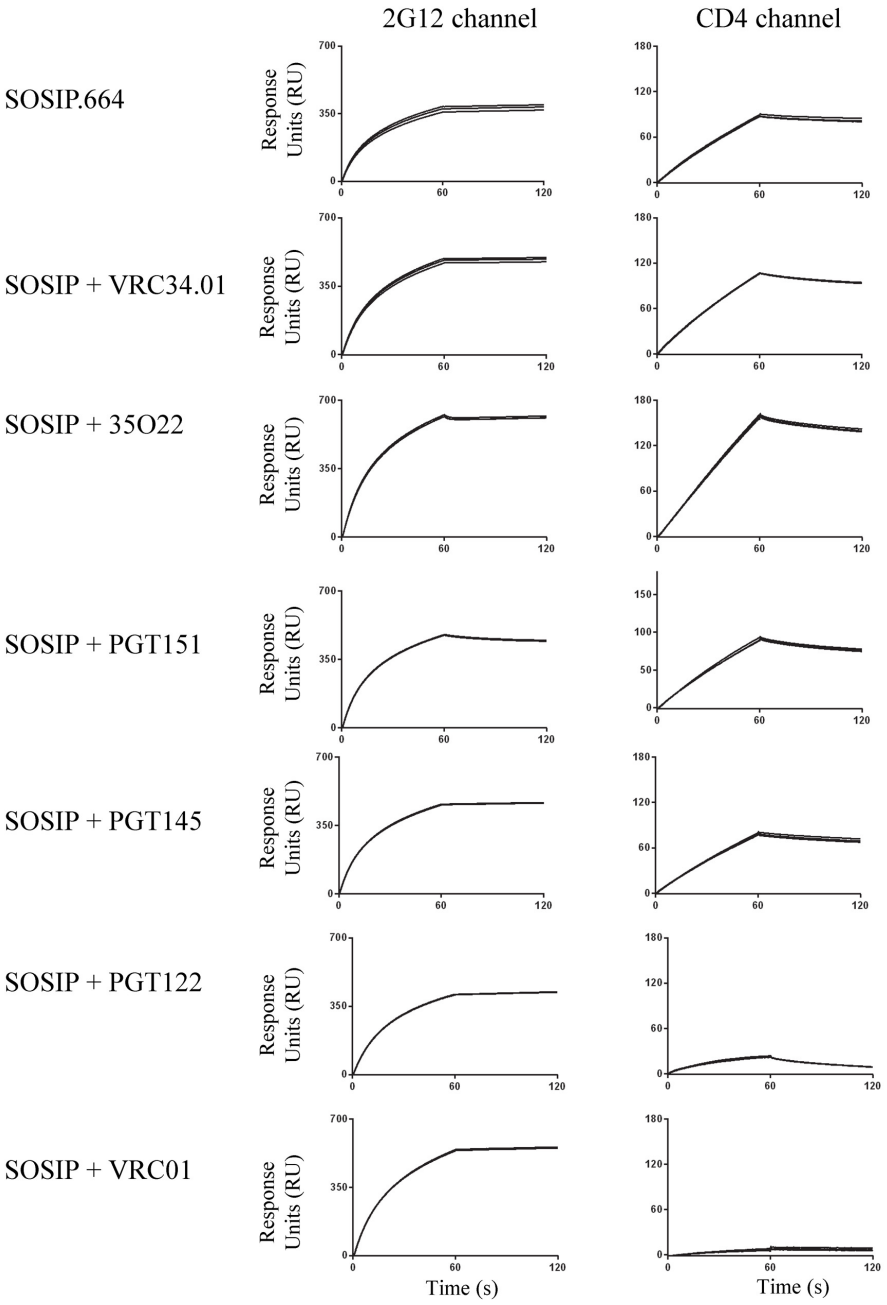

Fig. S15. Antibody inhibition of SOSIP.664 binding to CD4. Surface plasmon resonance measurement of SOSIP.664 binding to either 2G12 or CD4-Ig, alone or in the presence of antibody Fab fragments. The trimers samples were injected over a 2G12-immobilized channel and a CD4 Ig- immobilized surface. Each injection was repeated three times, and all three replicate sensorgrams are shown for each set of measurements. The response units were read out 60s post injection stop and the average responses were used to calculate the binding ratios reported in Figure 3C.

Neutralization IC_{50} (µg/ml) against HIV-1 JR-FL.JB	
CD4-Ig	0.3
VRC01	0.05
10E8	0.5
VRC34.01	0.19
PGT151	0.01
35O22	0.01
PG9	0.5
PGT128	0.01
PGT121	0.04

Fig. S16. Neutralization IC_{50} (µg/ml) of the single-round of replication Env-pseudotyped JR-FL.JB virus on in TZM-bl target cells by multiple mAbs.

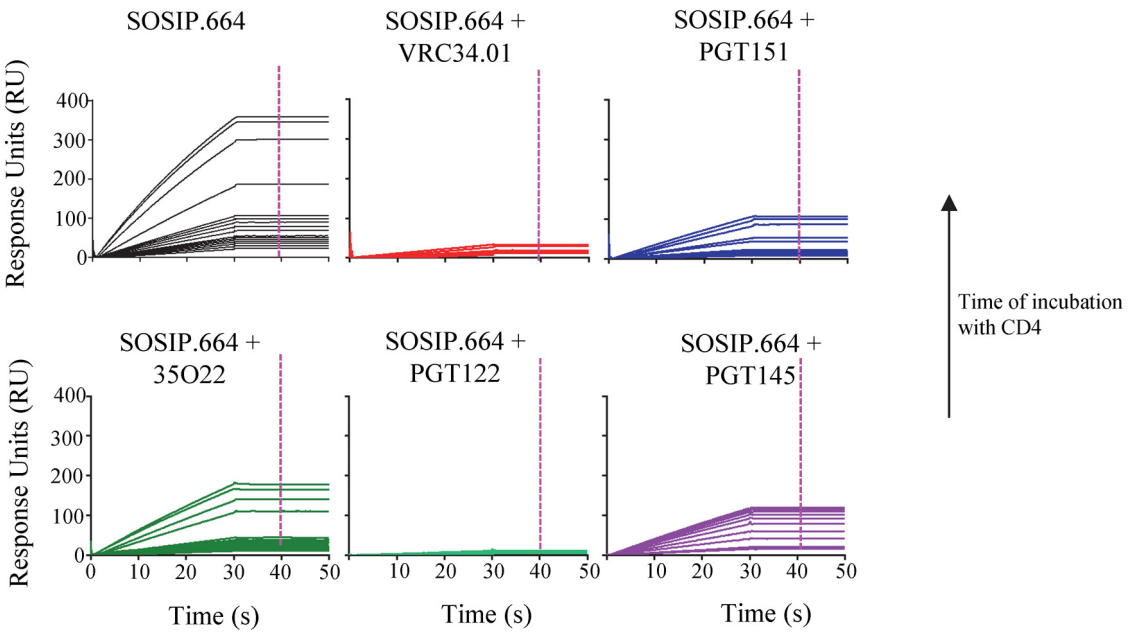

Fig. S17. Inhibition of CD4-induced activation of SOSIP.664 by antibodies VRC34.01, PGT151, 35O22, PGT122 and PGT145. Samples containing SOSIP.664, either alone or in the presence of antibody Fab fragments, incubated with soluble, 2-domain CD4, were injected onto a 17b antibody surface at different time-points. Each line on a graph indicates a double referenced sensorgram from an independent sample injection at a time-point, color-coded by antibody using the color scheme depicted in Figure 3. The vertical, dotted magenta line indicates the time-points at which the response units are reported in Figure 3. Experiments were replicated at least three times and representative datasets are show

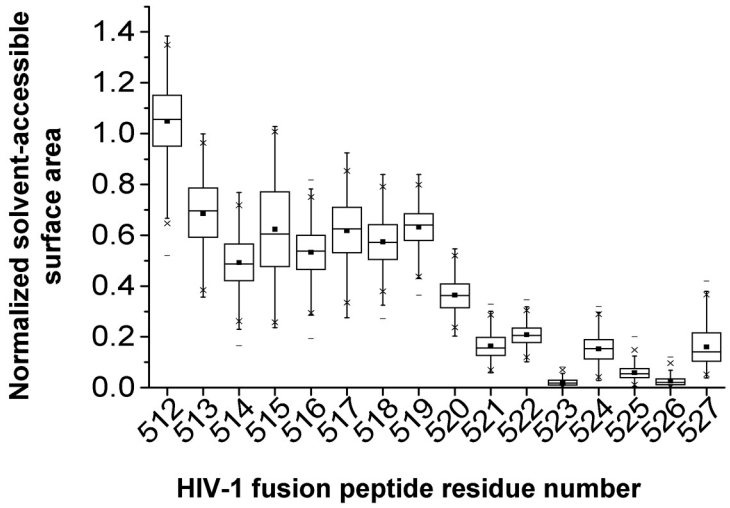

Fig. S18. Simulation reveals residues 512-520 of the fusion peptide are solvent exposed. Box-and-whisker plot for normalized solvent-accessible surface area (SASA) over 500 ns of molecular dynamics simulation. The median normalized SASA value for each residue is represented as horizontal line in each box. The mean value is represented as a small filled box. The height of each box is set by the 25th and 75th interquartile range and the whiskers are determined by the 5th and 95th percentiles. The minimum and maximum normalized SASA value for each residue over the length of the simulation is represented as 'x.' All SASA values from the fusion peptide were normalized using a fully extended Gly-Xxx-Gly peptide (where Xxx is the residue under consideration). The normalized SASA value for residue 512 can be larger than 1.0 since the n-terminus of this residue is completely exposed.

A

Construct Name	ELISA binding to VRC34.01
Pep1-1y12-cHis_pVRC8400	0.0477
Pep1-2-1y12-cHis_pVRC8400	0.0543
Pep1-1y12-Gly1-cHis_pVRC8400	0.0486
Pep1-1y12-Gly2-cHis_pVRC8400	0.0518
Pep1-1y12-Gly1-2-cHis_pVRC8400	0.0458
Pep1-2-1y12-Gly1-cHis_pVRC8400	0.0559
Pep1-2-1y12-Gly2-cHis_pVRC8400	0.0658
Pep1-2-1y12-Gly1-2-cHis_pVRC8400	0.0499
Pep1-1y12-cHis-R157c-g90c_pVRC8400	1.2992
Pep1-2-1y12-cHis-R157c-g90c_pVRC8400	0.065
Pep1-1y12-Gly1-cHis-R157c-g90c_pVRC8400	0.0509
Pep1-1y12-Gly2-cHis-R157c-g90c_pVRC8400	1.4213
Pep1-1y12-Gly1-2-cHis-R157c-g90c_pVRC8400	0.1231
Pep1-2-1y12-Gly1-cHis-R157c-g90c_pVRC8400	0.0531
Pep1-2-1y12-Gly2-cHis-R157c-g90c_pVRC8400	0.0759
Pep1-2-1y12-Gly1-2-cHis-R157c-g90c_pVRC8400	0.0558
Pep1_Ferr-His06_pVRC8400	0.0518
Pep1-2_Ferr-His06_pVRC8400	0.049
Pep1_Ferr-His06-gly1_pVRC8400	0.0465
Pep1_Ferr-His06-gly2_pVRC8400	0.0498
Pep1-2_Ferr-His06-gly1_pVRC8400	0.0492
Pep1-2_Ferr-His06-gly2_pVRC8400	0.0545
Pep1-2_Ferr-His06-gly1-2_pVRC8400	0.0501
FP_glyc88_1Q2N_trunc1-4_K7N_Q9T_gyc_pVRC8400	2.2821
FP_glyc88_1Q2N_trunc1-4_Q10N_A12S_gyc_pVRC8400	2.1907
FP_glyc88_1Q2N_trunc1-4_K35N_D37T_gyc_pVRC8400	1.0262
FP_glyc88_1Q2N_trunc1-4_N39S_gyc_pVRC8400	0.048
FP_glyc88_1CEI_trunc3-5_K43N_gyc_pVRC8400	0.1797
FP_glyc88_1CEI_trunc3-5_V33N_D35T_gyc_pVRC8400	0.0581
FP_glyc88_1CEI_trunc3-5_E21N_E23T_gyc_pVRC8400	0.0565
FP_glyc88_1M6T_A35N_A37S_gyc_pVRC8400	2.8017
FP_glyc88_1M6T_K42N_gyc_pVRC8400	2.8479
FP_glyc88_1M6T_E49N_K51T_gyc_pVRC8400	2.7248
FP_glyc88_1AAP_trunc1-3_E7N_A9S_gyc_pVRC8400	0.0677
FP_glyc88_1AAP_trunc1-3_R42N_N44T_gyc_pVRC8400	0.0493
FP_glyc88_1FNA_trunc1-5_E9N_V11T_gyc_pVRC8400	1.0919
FP_glyc88_1FNA_trunc1-5_A26N_gyc_pVRC8400	0.0545
FP_glyc88_1CBH_S21N_gyc_pVRC8400	0.054
No DNA	0.0536

B

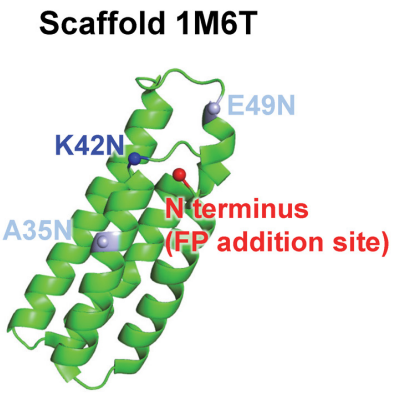

C

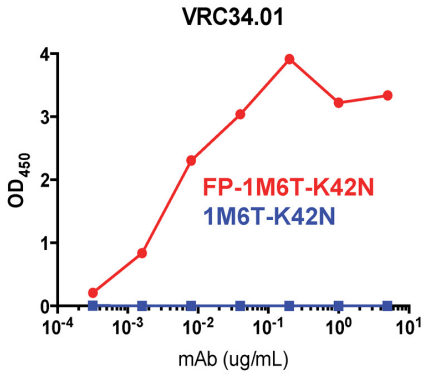

Fig. S19. VRC34-epitope scaffold design. (A) Construct names and ELISA signals for VRC34.01 binding in a 96-well transfection format. (B) The structure of the scaffold used for the top 3 designs. The N-terminus of the scaffold, where the fusion peptide were added to via a GCG linker, is shown in red. The sites where N-linked glycosylation were introduced are shown in blue (K42N) or light blue (A35N, E49N). (C) ELISA analysis of the 1M6T-K42N scaffolds, with and without attaching the fusion peptide at the N-terminus, with VRC34.01.

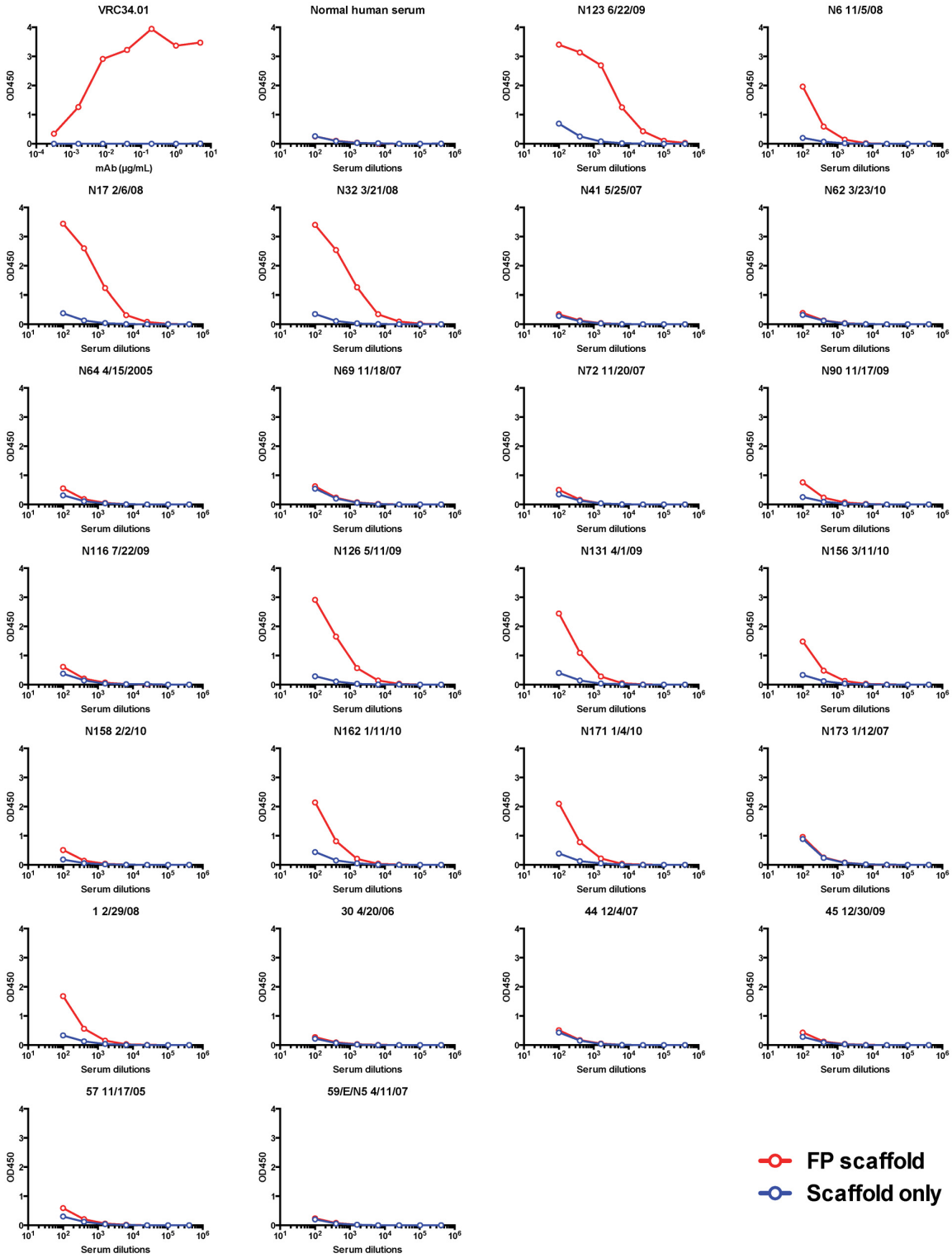
VRC34.01
Normal human serum
N123 6/22/09
N6 11/5/08
N17 2/6/08
N32 3/21/08
N41 5/25/07
N62 3/23/10
N64 4/15/2005
N69 11/18/07
N72 11/20/07
N90 11/17/09
N116 7/22/09
N126 5/11/09
N131 4/1/09
N156 3/11/10
N158 2/2/10
N162 1/11/10
N171 1/4/10
N173 1/12/07
1 2/29/08
30 4/20/06
44 12/4/07
45 12/30/09
57 11/17/05
59/E/N5 4/11/07
OD450
mAb (µg/mL)
Serum dilutions
FP scaffold
Scaffold only

Fig. S20. Serum binding to fusion peptide in ELISA. 24 sera from a NIAID cohort of HIV-1 infected subjects were assessed in ELISA for binding to a VRC34-epitope scaffold protein with BG505 fusion peptide 512-519 sequence (red line) or the control scaffold only (blue line). mAb VRC34.01 and a normal human serum were tested as control.

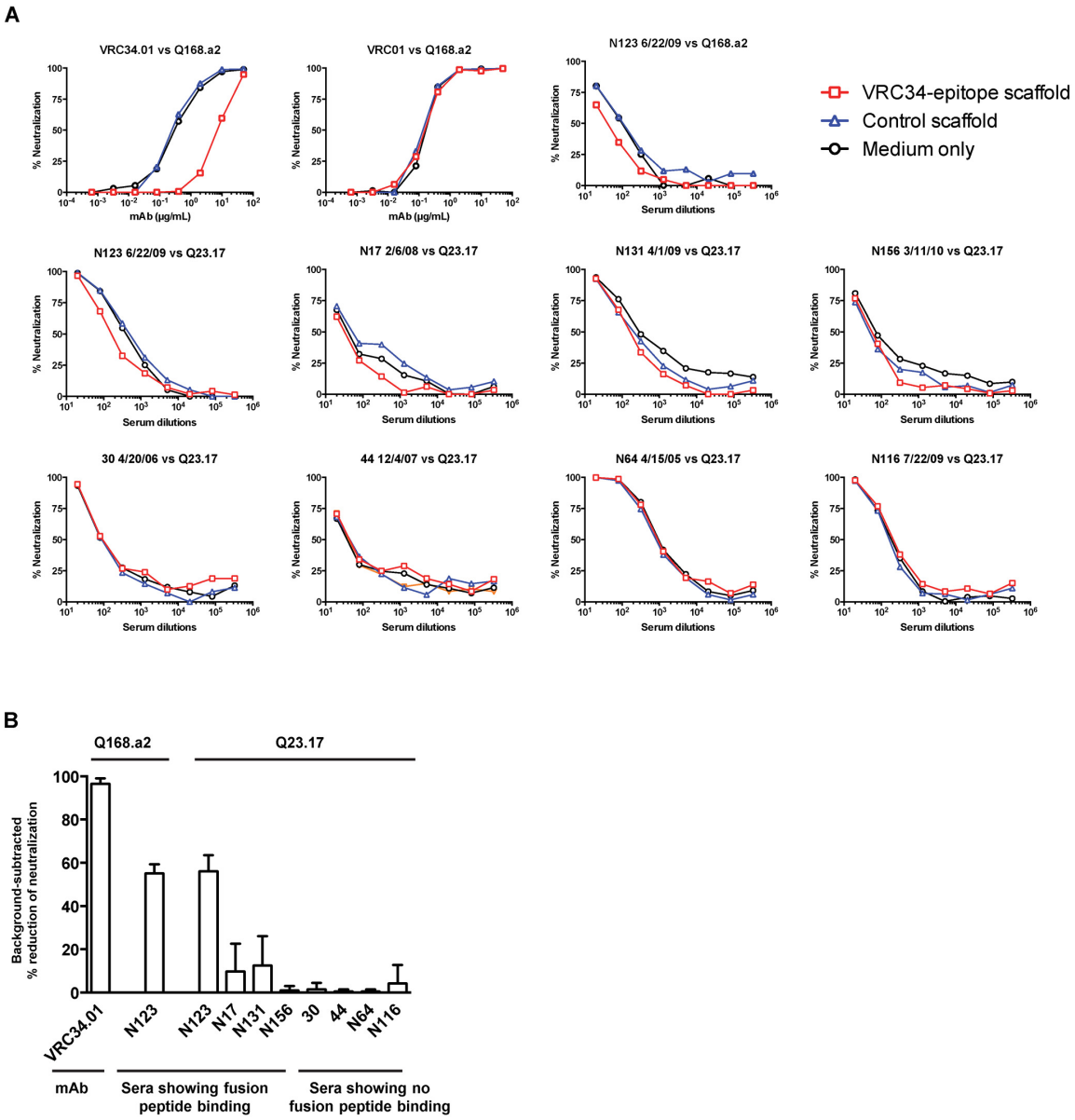

Fig. S21. mAb and serum neutralization in the presence of VRC34-epitope scaffold. (A) Neutralization curves of mAbs and serum in the presence of VRC34-epitope scaffold, control scaffold or medium. One representative of four independent experiments is shown. (B) Percent reduction of serum neutralization against HIV-1 Q168.a2 and Q23.17 in the presence of VRC34-epitope scaffold. As described in methods, the percent reduction in the presence of VRC34-epitope scaffold is calculated by comparing to the presence of control scaffold. Mean and standard deviation (SD) of four independent experiments are shown.

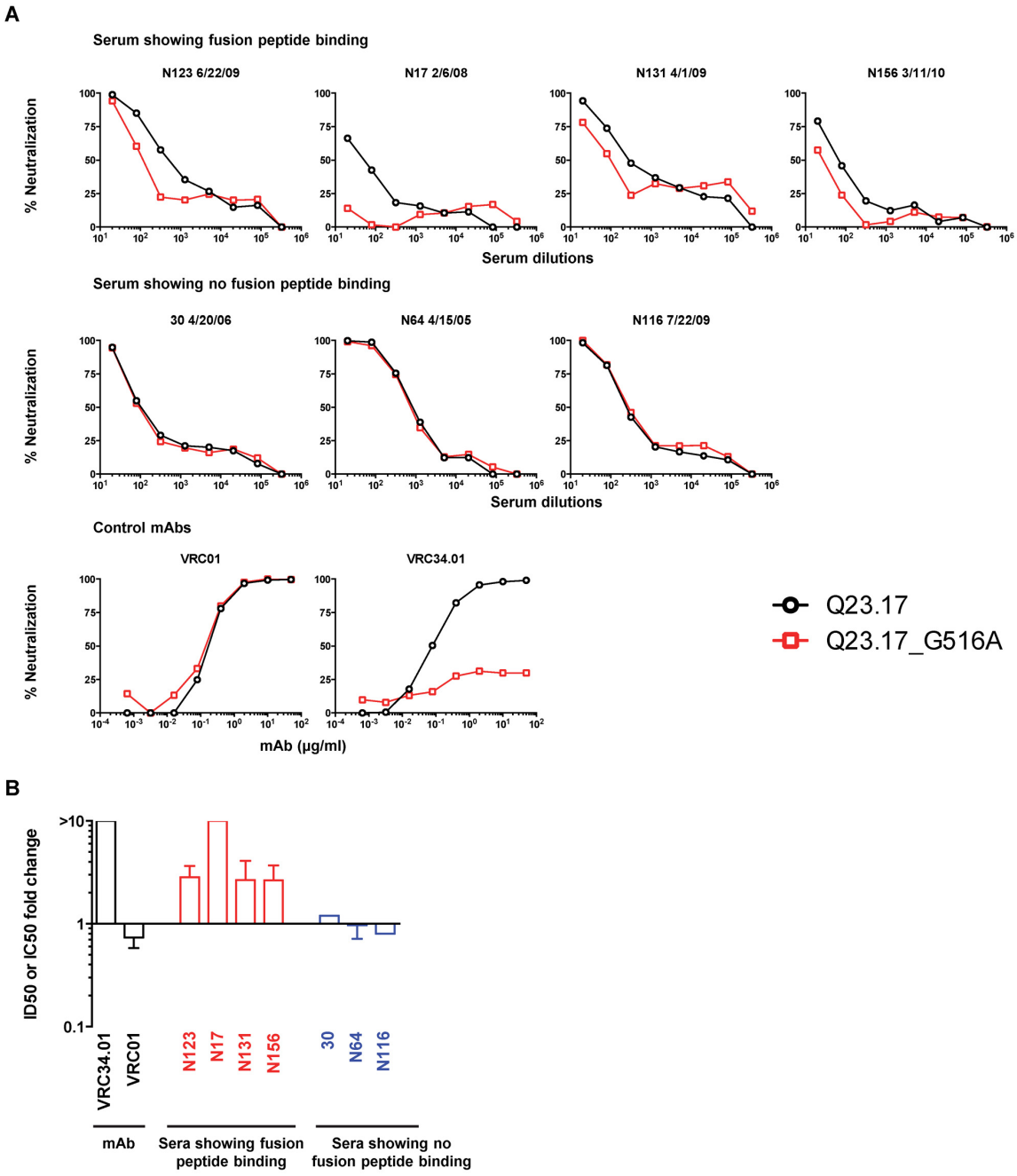

Fig. S22. mAb and serum neutralization against wildtype Q23.17 and fusion peptide mutant viruses. (A) mAb and serum neutralization against wildtype Q23.17 and G516A mutant. One representative of three independent experiments is shown. (B) Neutralization ID_{50} or IC_{50} fold change of mAb and serum against wildtype Q23.17 and G516A mutant. A value of 1 indicates no change, while >1 indicates reduced neutralizing activity and <1 indicates enhanced neutralizing activity. When the neutralizing activity was knocked out by the mutation, the ID_{50} or IC_{50} change is shown as >10. Mean and standard deviation (SD) of three independent experiments are shown.

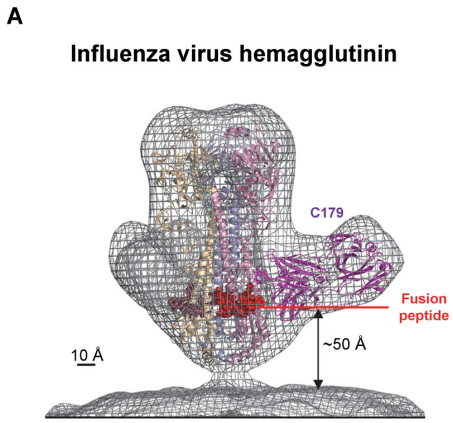

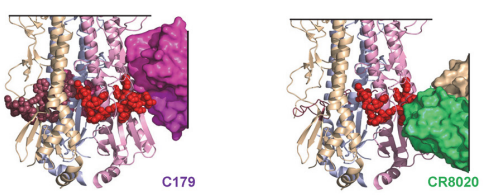

C

1-GLFGAIAGFIEGGWQGMVDGWYG-23

		Q	G	M	V	D	G	W
mAb ASA (Å²)	C179	0.0	0.0	0.1	17.2	61.3	9.1	32.1
	CR8020	77.4	49.5	0.0	95.1	90.8	0.0	0.0
Total ASA (Å²)		177.6	53.2	23.0	131.5	119.1	17.4	159.1

Fig. S23. Antibody recognition of influenza hemagglutinin fusion peptide. (A) Fab C179 bound to H2N2 hemagglutinin (PDB 4HLZ) is shown in ribbon representation with fusion peptide (1-23) in red spheres docked into the cryo-EM map (EMDB 5684; gray mesh) of influenza hemagglutinin bound by antibody C179. Similar to respiratory syncytial virus (RSV) fusion glycoprotein (*65*), the fusion peptide of influenza virus hemagglutinin (*66, 67*) reside ~50 Å from the membrane. (B) Zoom-in of influenza hemagglutinin fusion peptide (red spheres) bound by neutralizing antibodies C179 (left) and CR8020 (right). With RSV, a conformational change after cleavage buries the fusion peptide (*65*), whereas with influenza, the fusion peptide is partially exposed and the primary difference with HIV-1 Env is that the N-terminus of the fusion peptide is fixed, and not free to move. Interestingly, broadly neutralizing antibodies (*68*) do recognize the influenza hemagglutinin fusion peptide. (C) Surface areas for influenza-neutralizing antibodies C179 and CR8020 with the influenza fusion peptide. Per residue-contact surface areas are shown along with the total accessible surface areas of these residues. Both HIV-1- and influenza-fusion peptide targeting antibodies trap the fusion machinery in a pre-fusion state. However, influenza antibodies target C-terminal portion of the fusion peptide, not its N-terminus, and influenza-neutralizing antibodies bind the hemagglutinin fusion peptide as a small component of their recognition, whereas VRC34.01 binds the HIV-1 Env fusion peptide as a dominant component of its recognition.

Table S1. Data collection and refinement statistics.

	Env/VRC34 Fab /PGT122 Fab complex	VRC34 Fab	Synthetic fusion peptide/VRC34 Fab
PDB accession codes	5I8H	5I8E	5I8C
Wavelength (Å)	1	1	1
Resolution range (Å)	50 - 4.3 (4.4 - 4.3)*	50 - 2.65 (2.75 - 2.65)	50 - 1.5 (1.6 - 1.5)
Space group	R 3_2: H	I 4	P 2_1 2_1 2_1
Unit cell	252.3 252.3 561.2 90 90 120	114.6 114.6 174.1 90 90 90	63.5 74.9 84.5 90 90 90
Total reflections	1,443,488	511,125	942,320
Unique reflections	39,396 (2329)	30,065 (3065)	60,166 (5841)
Multiplicity	4.6 (4.2)	3.3 (3.3)	7.1 (5.3)
Completeness (%)	82.7 (49.7)	92.9 (94.4)	99.7 (97.9)
I*/σ*I	5.4 (1.1)	10.2 (2.6)	29.4 (14.1)
Wilson B-factor (Å^2)	174	65	9.5
R_{merge} [a]	0.132 (0.903)	0.123 (0.807)	0.066 (0.140)
R_{pim} [b]	0.063 (0.435)	0.026 (0.066)	0.072 (0.484)
$CC_{1/2}$ [c]	0.82	0.57	0.98
R_{work} [d]	0.27 (0.42)	0.19 (0.30)	0.159 (0.160)
R_{free} [d]	0.32 (0.41)	0.25 (0.42)	0.181 (0.211)
Number of non-hydrogen atoms	23988	6546	4112
macromolecules	22452	6411	3353
ligands	1536	10	
water	0	125	759
Protein residues	2974	846	443
RMS(bonds)	0.005	0.01	0.007
RMS(angles)	0.95	1.53	1.19
Ramachandran favored (%)	92	95	98
Ramachandran outliers (%)	0.98	0.72	0
Clashscore	9.99	12.46	2.56
Average B-factor	243	82	14
macromolecules	242	83	11
ligands	261	85	
solvent		63	25

* Statistics for the highest-resolution shell are shown in parentheses.

[a] $R_{merge} = \Sigma_{hkl}|I - \langle I \rangle| / \Sigma I_{hkl}$, where I is the observed intensity for a reflection and $\langle I \rangle$ is the average intensity of a unique reflection obtained from symmetry-related and multiple measurements.

[b] R_{pim} is the precision-indicating (multiplicity-weighted) R_{merge}.

[c] $CC_{1/2}$ is the percentage of correlation between intensities from random half-datasets.

[d] $R = \Sigma_{hkl}||F_{obs}| - |F_{calc}|| / \Sigma_{hkl}|F_{obs}|$, where F_{calc} and F_{obs} are calculated and observed structure factor amplitudes, respectively. R_{free} was calculated as R_{work} using 5% of reflections excluded in refinement. R_{work} is calculated for the remaining reflections.

Table S2. Surface areas of interaction for VRC34.01 in ternary complex with PGT122 and BG505 SOSIP.664 trimer.

HIV-1 Env region	Buried surface area (Å^2)			% Total
	Heavy Chain	Light Chain	Total	
Fusion peptide	562	194	756	54.7
Glycan-88	131	229	360	26.0
Other	267	0	267	19.3
Total	960	423	1383	100.0

Table S3. IC_{50} and IC_{80} values of mAb neutralization against JR-FL in different assay format.

	Unwashed		Washed		Fold change[b]	
	IC_{50}	IC_{80}	IC_{50}	IC_{80}	IC_{50}	IC_{80}
VRC34.01	0.19 ± 0.04[a]	0.84 ± 0.21	0.54 ± 0.25	2.56 ± 0.71	2.86 ± 1.30	3.06 ± 0.59
b12	0.04 ± 0.01	0.12 ± 0.03	0.16 ± 0.10	0.31 ± 0.10	4.66 ± 3.45	2.76 ± 1.33
4E10	6.59 ± 1.89	18.38 ± 2.73	>50	>50	N/A	N/A

[a] Mean and standard deviation of three independent experiments are shown.
[b] IC_{50} and IC_{80} fold change of washed versus unwashed neutralization assay.

Online supplementary files

Database S1.
Antibody neutralization data against 208 HIV-1 Env-pseudoviruses.

Database S2
Fusion peptide sequence analysis and VRC34.01 neutralization of 208 HIV-1 strains presented in Figure 2B and 2D.

Database S3
Sequences of VRC34-epitope scaffold designs presented in Figure S19.

References

1. P. M. Colman, M. C. Lawrence, The structural biology of type I viral membrane fusion. *Nat. Rev. Mol. Cell Biol.* **4**, 309–319 (2003). Medline doi:10.1038/nrm1076

2. D. M. Eckert, P. S. Kim, Mechanisms of viral membrane fusion and its inhibition. *Annu. Rev. Biochem.* **70**, 777–810 (2001). Medline doi:10.1146/annurev.biochem.70.1.777

3. S. C. Harrison, Viral membrane fusion. *Nat. Struct. Mol. Biol.* **15**, 690–698 (2008). Medline doi:10.1038/nsmb.1456

4. J. P. Julien, A. Cupo, D. Sok, R. L. Stanfield, D. Lyumkis, M. C. Deller, P. J. Klasse, D. R. Burton, R. W. Sanders, J. P. Moore, A. B. Ward, I. A. Wilson, Crystal structure of a soluble cleaved HIV-1 envelope trimer. *Science* **342**, 1477–1483 (2013). Medline doi:10.1126/science.1245625

5. D. Lyumkis, J. P. Julien, N. de Val, A. Cupo, C. S. Potter, P. J. Klasse, D. R. Burton, R. W. Sanders, J. P. Moore, B. Carragher, I. A. Wilson, A. B. Ward, Cryo-EM structure of a fully glycosylated soluble cleaved HIV-1 envelope trimer. *Science* **342**, 1484–1490 (2013). Medline doi:10.1126/science.1245627

6. M. Pancera, T. Zhou, A. Druz, I. S. Georgiev, C. Soto, J. Gorman, J. Huang, P. Acharya, G. Y. Chuang, G. Ofek, G. B. Stewart-Jones, J. Stuckey, R. T. Bailer, M. G. Joyce, M. K. Louder, N. Tumba, Y. Yang, B. Zhang, M. S. Cohen, B. F. Haynes, J. R. Mascola, L. Morris, J. B. Munro, S. C. Blanchard, W. Mothes, M. Connors, P. D. Kwong, Structure and immune recognition of trimeric pre-fusion HIV-1 Env. *Nature* **514**, 455–461 (2014). Medline doi:10.1038/nature13808

7. Y. D. Kwon, M. Pancera, P. Acharya, I. S. Georgiev, E. T. Crooks, J. Gorman, M. G. Joyce, M. Guttman, X. Ma, S. Narpala, C. Soto, D. S. Terry, Y. Yang, T. Zhou, G. Ahlsen, R. T. Bailer, M. Chambers, G. Y. Chuang, N. A. Doria-Rose, A. Druz, M. A. Hallen, A. Harned, T. Kirys, M. K. Louder, S. O'Dell, G. Ofek, K. Osawa, M. Prabhakaran, M. Sastry, G. B. Stewart-Jones, J. Stuckey, P. V. Thomas, T. Tittley, C. Williams, B. Zhang, H. Zhao, Z. Zhou, B. R. Donald, L. K. Lee, S. Zolla-Pazner, U. Baxa, A. Schön, E. Freire, L. Shapiro, K. K. Lee, J. Arthos, J. B. Munro, S. C. Blanchard, W. Mothes, J. M. Binley, A. B. McDermott, J. R. Mascola, P. D. Kwong, Crystal structure, conformational fixation and entry-related interactions of mature ligand-free HIV-1 Env. *Nat. Struct. Mol. Biol.* **22**, 522–531 (2015). Medline doi:10.1038/nsmb.3051

8. N. A. Doria-Rose, R. M. Klein, M. G. Daniels, S. O'Dell, M. Nason, A. Lapedes, T. Bhattacharya, S. A. Migueles, R. T. Wyatt, B. T. Korber, J. R. Mascola, M. Connors, Breadth of human immunodeficiency virus-specific neutralizing activity in sera: Clustering analysis and association with clinical variables. *J. Virol.* **84**, 1631–1636 (2010). Medline doi:10.1128/JVI.01482-09

9. N. A. Doria-Rose, R. M. Klein, M. M. Manion, S. O'Dell, A. Phogat, B. Chakrabarti, C. W. Hallahan, S. A. Migueles, J. Wrammert, R. Ahmed, M. Nason, R. T. Wyatt, J. R. Mascola, M. Connors, Frequency and phenotype of human immunodeficiency virus envelope-specific B cells from patients with broadly cross-neutralizing antibodies. *J. Virol.* **83**, 188–199 (2009). Medline doi:10.1128/JVI.01583-08

10. R. W. Sanders, R. Derking, A. Cupo, J. P. Julien, A. Yasmeen, N. de Val, H. J. Kim, C. Blattner, A. T. de la Peña, J. Korzun, M. Golabek, K. de Los Reyes, T. J. Ketas, M. J. van

Gils, C. R. King, I. A. Wilson, A. B. Ward, P. J. Klasse, J. P. Moore, A next-generation cleaved, soluble HIV-1 Env trimer, BG505 SOSIP.664 gp140, expresses multiple epitopes for broadly neutralizing but not non-neutralizing antibodies. *PLOS Pathog.* **9**, e1003618 (2013). Medline doi:10.1371/journal.ppat.1003618

11. D. Sok, M. J. van Gils, M. Pauthner, J. P. Julien, K. L. Saye-Francisco, J. Hsueh, B. Briney, J. H. Lee, K. M. Le, P. S. Lee, Y. Hua, M. S. Seaman, J. P. Moore, A. B. Ward, I. A. Wilson, R. W. Sanders, D. R. Burton, Recombinant HIV envelope trimer selects for quaternary-dependent antibodies targeting the trimer apex. *Proc. Natl. Acad. Sci. U.S.A.* **111**, 17624–17629 (2014). Medline doi:10.1073/pnas.1415789111

12. C. Blattner, J. H. Lee, K. Sliepen, R. Derking, E. Falkowska, A. T. de la Peña, A. Cupo, J. P. Julien, M. van Gils, P. S. Lee, W. Peng, J. C. Paulson, P. Poignard, D. R. Burton, J. P. Moore, R. W. Sanders, I. A. Wilson, A. B. Ward, Structural delineation of a quaternary, cleavage-dependent epitope at the gp41-gp120 interface on intact HIV-1 Env trimers. *Immunity* **40**, 669–680 (2014). Medline

13. E. Falkowska, K. M. Le, A. Ramos, K. J. Doores, J. H. Lee, C. Blattner, A. Ramirez, R. Derking, M. J. van Gils, C. H. Liang, R. Mcbride, B. von Bredow, S. S. Shivatare, C. Y. Wu, P. Y. Chan-Hui, Y. Liu, T. Feizi, M. B. Zwick, W. C. Koff, M. S. Seaman, K. Swiderek, J. P. Moore, D. Evans, J. C. Paulson, C. H. Wong, A. B. Ward, I. A. Wilson, R. W. Sanders, P. Poignard, D. R. Burton, Broadly neutralizing HIV antibodies define a glycan-dependent epitope on the prefusion conformation of gp41 on cleaved envelope trimers. *Immunity* **40**, 657–668 (2014). Medline

14. L. M. Walker, M. Huber, K. J. Doores, E. Falkowska, R. Pejchal, J. P. Julien, S. K. Wang, A. Ramos, P. Y. Chan-Hui, M. Moyle, J. L. Mitcham, P. W. Hammond, O. A. Olsen, P. Phung, S. Fling, C. H. Wong, S. Phogat, T. Wrin, M. D. Simek, W. C. Koff, I. A. Wilson, D. R. Burton, P. Poignard; Protocol G Principal Investigators, Broad neutralization coverage of HIV by multiple highly potent antibodies. *Nature* **477**, 466–470 (2011). Medline doi:10.1038/nature10373

15. A. J. McCoy, R. W. Grosse-Kunstleve, P. D. Adams, M. D. Winn, L. C. Storoni, R. J. Read, Phaser crystallographic software. *J. Appl. Crystallogr.* **40**, 658–674 (2007). Medline doi:10.1107/S0021889807021206

16. Residue number for HIV-1 Env follows the standard HXB2 convention (www.hiv.lanl.gov/content/sequence/HIV/REVIEWS/HXB2.html).

17. VRC34.01-bound portions of fusion peptide (residues 512 to 517) were disordered in previous HIV-1 Env structures, whereas residues 518 to 530 were ordered in the PGT122-35O22–bound HIV-1 structure (PDB ID 4TVP) and assumed the same conformation as in the VRC34.01-bound structure (0.19 Å root mean square deviation).

18. Residues 512 to 519 (which correspond to the N terminus of the fusion peptide and are recognized by VRC34.01) do not interact with other portions of the HIV-1 Env. Residues 520 to 530 of the fusion peptide are embedded in a groove defined by gp41 residues 533 to 543 and 627 and by gp120 residues 45, 84 to 89, 492, and glycan N88.

19. Antibody residue numbers follow Kabat convention, and, for clarity, heavy-chain residues are followed by an “HC” subscript and light-chain residues by an “LC” subscript. In some cases, the CDR loops are specified to provide further clarity.

20. The pocket for A512 is defined by $E32_{CDR\ L1}$, $M91_{CDR\ L3}$, $E100^{A}_{CDR\ H3}$, and $A100^{B}_{CDR\ H3}$; the pocket for V513 is defined by $S93_{CDR\ L3}$, $Y94_{CDR\ L3}$, $W50_{CDR\ H2}$, and $A100^{B}_{CDR\ H3}$; the pocket for I515 is defined by $A33_{CDR\ H1}$, $W50_{CDR\ H2}$, $I51_{CDR\ H2}$, $N52_{CDR\ H2}$, and $Y97_{CDR\ H3}$; and the pocket for V518 is defined by $G31_{CDR\ H1}$, $N52_{CDR\ H2}$, and $Y97_{CDR\ H3}$.

21. J. Huang, B. H. Kang, M. Pancera, J. H. Lee, T. Tong, Y. Feng, H. Imamichi, I. S. Georgiev, G. Y. Chuang, A. Druz, N. A. Doria-Rose, L. Laub, K. Sliepen, M. J. van Gils, A. T. de la Peña, R. Derking, P. J. Klasse, S. A. Migueles, R. T. Bailer, M. Alam, P. Pugach, B. F. Haynes, R. T. Wyatt, R. W. Sanders, J. M. Binley, A. B. Ward, J. R. Mascola, P. D. Kwong, M. Connors, Broad and potent HIV-1 neutralization by a human antibody that binds the gp41-gp120 interface. *Nature* **515**, 138–142 (2014). Medline doi:10.1038/nature13601

22. Sequences of 3943 HIV-1 strains were downloaded from the HIV database (www.hiv.lanl.gov/content/index).

23. P. D. Kwong, M. L. Doyle, D. J. Casper, C. Cicala, S. A. Leavitt, S. Majeed, T. D. Steenbeke, M. Venturi, I. Chaiken, M. Fung, H. Katinger, P. W. Parren, J. Robinson, D. Van Ryk, L. Wang, D. R. Burton, E. Freire, R. Wyatt, J. Sodroski, W. A. Hendrickson, J. Arthos, HIV-1 evades antibody-mediated neutralization through conformational masking of receptor-binding sites. *Nature* **420**, 678–682 (2002). Medline doi:10.1038/nature01188

24. J. B. Munro, J. Gorman, X. Ma, Z. Zhou, J. Arthos, D. R. Burton, W. C. Koff, J. R. Courter, A. B. Smith 3rd, P. D. Kwong, S. C. Blanchard, W. Mothes, Conformational dynamics of single HIV-1 envelope trimers on the surface of native virions. *Science* **346**, 759–763 (2014). Medline doi:10.1126/science.1254426

25. The following nomenclature is used: “Tolerated” Env sequences contained one or more mutations within the eight residue fusion-peptide sequence, which individually showed little effect on VRC34.01 neutralization. “Affected” sequences contained one or more residues (513I, 513A, 514b_T, 515M, 518M, 518L, 519I, or 519L) that diminished VRC34.01 neutralization. “Untested” sequences contained one or more untested residues plus tolerated residues.

26. P. D. Kwong, R. Wyatt, J. Robinson, R. W. Sweet, J. Sodroski, W. A. Hendrickson, Structure of an HIV gp120 envelope glycoprotein in complex with the CD4 receptor and a neutralizing human antibody. *Nature* **393**, 648–659 (1998). Medline doi:10.1038/31405

27. A. Trkola, T. Dragic, J. Arthos, J. M. Binley, W. C. Olson, G. P. Allaway, C. Cheng-Mayer, J. Robinson, P. J. Maddon, J. P. Moore, CD4-dependent, antibody-sensitive interactions between HIV-1 and its co-receptor CCR-5. *Nature* **384**, 184–187 (1996). Medline doi:10.1038/384184a0

28. J. Liu, A. Bartesaghi, M. J. Borgnia, G. Sapiro, S. Subramaniam, Molecular architecture of native HIV-1 gp120 trimers. *Nature* **455**, 109–113 (2008). Medline doi:10.1038/nature07159

29. M. J. Harvey, G. Giupponi, G. D. Fabritiis, ACEMD: Accelerating biomolecular dynamics in the microsecond time scale. *J. Chem. Theory Comput.* **5**, 1632–1639 (2009). Medline doi:10.1021/ct9000685

30. While 500 ns is not enough time to sample large-scale conformational transitions associated with the prefusion HIV-1 Env trimer, it should be sufficient to assess local motions of the fusion peptide.

31. When trimers are positioned into nearest-neighbor contact, only the N-terminal three residues of the fusion peptide can extend to contact a fusion peptide on a neighboring trimer. The N-terminal three residues of the fusion peptide are Ala-Val-Gly. Although the Ala-Val are somewhat hydrophobic, the positive charges of two N termini likely repel, preventing aggregation. In terms of close-by glycans, these may help to prevent aggregation, especially glycans N88, N611, and N618. However, it appears to be primarily the recessed nature of the fusion peptide, coupled to the fact that only eight residues of the fusion peptide are flexible (Fig. 4), that prevents aggregation.

32. Materials and methods are available as supplementary materials on *Science* Online.

33. M. Pancera, S. Shahzad-Ul-Hussan, N. A. Doria-Rose, J. S. McLellan, R. T. Bailer, K. Dai, S. Loesgen, M. K. Louder, R. P. Staupe, Y. Yang, B. Zhang, R. Parks, J. Eudailey, K. E. Lloyd, J. Blinn, S. M. Alam, B. F. Haynes, M. N. Amin, L. X. Wang, D. R. Burton, W. C. Koff, G. J. Nabel, J. R. Mascola, C. A. Bewley, P. D. Kwong, Structural basis for diverse N-glycan recognition by HIV-1-neutralizing V1-V2-directed antibody PG16. *Nat. Struct. Mol. Biol.* **20**, 804–813 (2013). Medline doi:10.1038/nsmb.2600

34. J. H. Lee, G. Ozorowski, A. B. Ward, Cryo-EM structure of a native, fully glycosylated, cleaved HIV-1 envelope trimer. *Science* **351**, 1043–1048 (2016). Medline doi:10.1126/science.aad2450

35. The structure of PGT151 in complex with HIV-1 Env was recently reported (*34*). This structure shows PGT151 to recognize the fusion peptide in an exposed, extended conformation.

36. Trimer (or trimer-antibody complex) was injected for 60 s onto CD4-IgG (immunoglobulin G) captured on a Biacore CM5 chip coated with a monoclonal mouse anti-human IgG (Fc) antibody (GE Healthcare), and binding responses were measured 60 s after the injection ended. Binding to CD4-Ig normalized with binding to antibody 2G12, which was measured similarly on a parallel-flow cell.

37. TZM-bl cells were incubated with JR-FL Env pseudovirus in the presence of antibodies at 50 μg/ml or medium control and then stained with biotinylated 2G12 followed by phycoerythrin (PE)–conjugated streptavidin. MFI was obtained from at least 10,000 cell events and normalized to the medium control.

38. The HIV Env trimer is conformationally dynamic. Binding and smFRET experiments show that VRC34 do not bind to the open co-receptor binding-competent conformation. Thus, any molecule spontaneously in that conformation would not be neutralized. The conformation specificity of VRC34.01 for the closed and intermediate conformation may explain the observed incomplete neutralization.

39. Specifically, soluble SOSIP.664 trimers were incubated with soluble, two-domain CD4, either alone or following preincubation with Fab, and the incubated trimer samples were injected over a 17b-coupled surface for 30 s, with response units reported 10 s after the injection ended.

40. X. Wu, Z. Y. Yang, Y. Li, C. M. Hogerkorp, W. R. Schief, M. S. Seaman, T. Zhou, S. D. Schmidt, L. Wu, L. Xu, N. S. Longo, K. McKee, S. O'Dell, M. K. Louder, D. L. Wycuff, Y. Feng, M. Nason, N. Doria-Rose, M. Connors, P. D. Kwong, M. Roederer, R. T. Wyatt, G. J. Nabel, J. R. Mascola, Rational design of envelope identifies broadly neutralizing human monoclonal antibodies to HIV-1. *Science* **329**, 856–861 (2010). Medline doi:10.1126/science.1187659

41. N. Doria-Rose, R. Bailer, M. Louder, C.-L. Lin, E. Turk, L. Laub, N. Longo, M. Connors, J. Mascola, High throughput HIV-1 microneutralization assay. *Protocol Exchange* **2013**, 10.1038/protex.2013.069 (2013).

42. M. Sarzotti-Kelsoe, R. T. Bailer, E. Turk, C. L. Lin, M. Bilska, K. M. Greene, H. Gao, C. A. Todd, D. A. Ozaki, M. S. Seaman, J. R. Mascola, D. C. Montefiori, Optimization and validation of the TZM-bl assay for standardized assessments of neutralizing antibodies against HIV-1. *J. Immunol. Methods* **409**, 131–146 (2014). Medline doi:10.1016/j.jim.2013.11.022

43. B. K. Chakrabarti, L. M. Walker, J. F. Guenaga, A. Ghobbeh, P. Poignard, D. R. Burton, R. T. Wyatt, Direct antibody access to the HIV-1 membrane-proximal external region positively correlates with neutralization sensitivity. *J. Virol.* **85**, 8217–8226 (2011). Medline doi:10.1128/JVI.00756-11

44. I. S. Georgiev, N. A. Doria-Rose, T. Zhou, Y. D. Kwon, R. P. Staupe, S. Moquin, G. Y. Chuang, M. K. Louder, S. D. Schmidt, H. R. Altae-Tran, R. T. Bailer, K. McKee, M. Nason, S. O'Dell, G. Ofek, M. Pancera, S. Srivatsan, L. Shapiro, M. Connors, S. A. Migueles, L. Morris, Y. Nishimura, M. A. Martin, J. R. Mascola, P. D. Kwong, Delineating antibody recognition in polyclonal sera from patterns of HIV-1 isolate neutralization. *Science* **340**, 751–756 (2013). Medline doi:10.1126/science.1233989

45. N. A. Doria-Rose, J. N. Bhiman, R. S. Roark, C. A. Schramm, J. Gorman, G. Y. Chuang, M. Pancera, E. M. Cale, M. J. Ernandes, M. K. Louder, M. Asokan, R. T. Bailer, A. Druz, I. R. Fraschilla, N. J. Garrett, M. Jarosinski, R. M. Lynch, K. McKee, S. O'Dell, A. Pegu, S. D. Schmidt, R. P. Staupe, M. S. Sutton, K. Wang, C. K. Wibmer, B. F. Haynes, S. Abdool-Karim, L. Shapiro, P. D. Kwong, P. L. Moore, L. Morris, J. R. Mascola, New member of the V1V2-directed CAP256-VRC26 lineage that shows increased breadth and exceptional potency. *J. Virol.* **90**, 76–91 (2015). Medline doi:10.1128/JVI.01791-15

46. N. A. Doria-Rose, C. A. Schramm, J. Gorman, P. L. Moore, J. N. Bhiman, B. J. DeKosky, M. J. Ernandes, I. S. Georgiev, H. J. Kim, M. Pancera, R. P. Staupe, H. R. Altae-Tran, R. T. Bailer, E. T. Crooks, A. Cupo, A. Druz, N. J. Garrett, K. H. Hoi, R. Kong, M. K. Louder, N. S. Longo, K. McKee, M. Nonyane, S. O'Dell, R. S. Roark, R. S. Rudicell, S. D. Schmidt, D. J. Sheward, C. Soto, C. K. Wibmer, Y. Yang, Z. Zhang, J. C. Mullikin, J. M. Binley, R. W. Sanders, I. A. Wilson, J. P. Moore, A. B. Ward, G. Georgiou, C. Williamson, S. S. Abdool Karim, L. Morris, P. D. Kwong, L. Shapiro, J. R. Mascola; NISC Comparative Sequencing Program, Developmental pathway for potent V1V2-directed HIV-neutralizing antibodies. *Nature* **509**, 55–62 (2014). Medline doi:10.1038/nature13036

47. X. Wu, A. B. Parast, B. A. Richardson, R. Nduati, G. John-Stewart, D. Mbori-Ngacha, S. M. Rainwater, J. Overbaugh, Neutralization escape variants of human immunodeficiency virus type 1 are transmitted from mother to infant. *J. Virol.* **80**, 835–844 (2006). Medline doi:10.1128/JVI.80.2.835-844.2006

48. J. S. McLellan, M. Pancera, C. Carrico, J. Gorman, J. P. Julien, R. Khayat, R. Louder, R. Pejchal, M. Sastry, K. Dai, S. O'Dell, N. Patel, S. Shahzad-ul-Hussan, Y. Yang, B. Zhang, T. Zhou, J. Zhu, J. C. Boyington, G. Y. Chuang, D. Diwanji, I. Georgiev, Y. D. Kwon, D. Lee, M. K. Louder, S. Moquin, S. D. Schmidt, Z. Y. Yang, M. Bonsignori, J. A. Crump, S. H. Kapiga, N. E. Sam, B. F. Haynes, D. R. Burton, W. C. Koff, L. M. Walker, S. Phogat, R. Wyatt, J. Orwenyo, L. X. Wang, J. Arthos, C. A. Bewley, J. R. Mascola, G. J. Nabel, W. R.

Schief, A. B. Ward, I. A. Wilson, P. D. Kwong, Structure of HIV-1 gp120 V1/V2 domain with broadly neutralizing antibody PG9. *Nature* **480**, 336–343 (2011). Medline doi:10.1038/nature10696

49. Z. Otwinowski, W. Minor, Processing of x-ray diffraction data collected in oscillation mode. *Methods Enzymol.* **276**, 307–326 (1997). doi:10.1016/S0076-6879(97)76066-X

50. P. D. Adams, K. Gopal, R. W. Grosse-Kunstleve, L. W. Hung, T. R. Ioerger, A. J. McCoy, N. W. Moriarty, R. K. Pai, R. J. Read, T. D. Romo, J. C. Sacchettini, N. K. Sauter, L. C. Storoni, T. C. Terwilliger, Recent developments in the PHENIX software for automated crystallographic structure determination. *J. Synchrotron Radiat.* **11**, 53–55 (2004). Medline doi:10.1107/S0909049503024130

51. P. Emsley, K. Cowtan, Coot: Model-building tools for molecular graphics. *Acta Crystallogr. D Biol. Crystallogr.* **60**, 2126–2132 (2004). Medline doi:10.1107/S0907444904019158

52. I. W. Davis, L. W. Murray, J. S. Richardson, D. C. Richardson, MOLPROBITY: Structure validation and all-atom contact analysis for nucleic acids and their complexes. *Nucleic Acids Res.* **32** (Web Server), W615–W619 (2004). Medline doi:10.1093/nar/gkh398

53. C. Suloway, J. Pulokas, D. Fellmann, A. Cheng, F. Guerra, J. Quispe, S. Stagg, C. S. Potter, B. Carragher, Automated molecular microscopy: The new Leginon system. *J. Struct. Biol.* **151**, 41–60 (2005). Medline doi:10.1016/j.jsb.2005.03.010

54. G. C. Lander, S. M. Stagg, N. R. Voss, A. Cheng, D. Fellmann, J. Pulokas, C. Yoshioka, C. Irving, A. Mulder, P. W. Lau, D. Lyumkis, C. S. Potter, B. Carragher, Appion: An integrated, database-driven pipeline to facilitate EM image processing. *J. Struct. Biol.* **166**, 95–102 (2009). Medline doi:10.1016/j.jsb.2009.01.002

55. G. Tang, L. Peng, P. R. Baldwin, D. S. Mann, W. Jiang, I. Rees, S. J. Ludtke, EMAN2: An extensible image processing suite for electron microscopy. *J. Struct. Biol.* **157**, 38–46 (2007). Medline doi:10.1016/j.jsb.2006.05.009

56. P. A. Penczek, R. A. Grassucci, J. Frank, The ribosome at improved resolution: New techniques for merging and orientation refinement in 3D cryo-electron microscopy of biological particles. *Ultramicroscopy* **53**, 251–270 (1994). Medline doi:10.1016/0304-3991(94)90038-8

57. E. F. Pettersen, T. D. Goddard, C. C. Huang, G. S. Couch, D. M. Greenblatt, E. C. Meng, T. E. Ferrin, UCSF Chimera—a visualization system for exploratory research and analysis. *J. Comput. Chem.* **25**, 1605–1612 (2004). Medline doi:10.1002/jcc.20084

58. R. B. Best, X. Zhu, J. Shim, P. E. Lopes, J. Mittal, M. Feig, A. D. Mackerell Jr., Optimization of the additive CHARMM all-atom protein force field targeting improved sampling of the backbone φ, ψ and side-chain χ_1 and χ_2 dihedral angles. *J. Chem. Theory Comput.* **8**, 3257–3273 (2012). Medline doi:10.1021/ct300400x

59. O. Guvench, S. S. Mallajosyula, E. P. Raman, E. Hatcher, K. Vanommeslaeghe, T. J. Foster, F. W. Jamison 2nd, A. D. Mackerell Jr., CHARMM additive all-atom force field for carbohydrate derivatives and its utility in polysaccharide and carbohydrate-protein modeling. *J. Chem. Theory Comput.* **7**, 3162–3180 (2011). Medline doi:10.1021/ct200328p

60. W. L. Jorgensen, J. Chandrasekhar, J. D. Madura, R. W. Impey, M. L. Klein, Comparison of simple potential functions for simulating liquid water. *J. Chem. Phys.* **79**, 926–935 (1983). doi:10.1063/1.445869

61. W. Wriggers, Using Situs for the integration of multi-resolution structures. *Biophys. Rev.* **2**, 21–27 (2010). Medline doi:10.1007/s12551-009-0026-3

62. F. Eisenhaber, P. Lijnzaad, P. Argos, C. Sander, M. Scharf, The double cubic lattice method: Efficient approaches to numerical integration of surface area and volume and to dot surface contouring of molecular assemblies. *J. Comput. Chem.* **16**, 273–284 (1995). doi:10.1002/jcc.540160303

63. R. Chu, J. Takei, J. R. Knowlton, M. Andrykovitch, W. Pei, A. V. Kajava, P. J. Steinbach, X. Ji, Y. Bai, Redesign of a four-helix bundle protein by phage display coupled with proteolysis and structural characterization by NMR and x-ray crystallography. *J. Mol. Biol.* **323**, 253–262 (2002). Medline doi:10.1016/S0022-2836(02)00884-7

64. M. Pancera, Y. Yang, M. K. Louder, J. Gorman, G. Lu, J. S. McLellan, J. Stuckey, J. Zhu, D. R. Burton, W. C. Koff, J. R. Mascola, P. D. Kwong, N332-Directed broadly neutralizing antibodies use diverse modes of HIV-1 recognition: Inferences from heavy-light chain complementation of function. *PLOS ONE* **8**, e55701 (2013). Medline doi:10.1371/journal.pone.0055701

65. J. S. McLellan, M. Chen, S. Leung, K. W. Graepel, X. Du, Y. Yang, T. Zhou, U. Baxa, E. Yasuda, T. Beaumont, A. Kumar, K. Modjarrad, Z. Zheng, M. Zhao, N. Xia, P. D. Kwong, B. S. Graham, Structure of RSV fusion glycoprotein trimer bound to a prefusion-specific neutralizing antibody. *Science* **340**, 1113–1117 (2013). Medline doi:10.1126/science.1234914

66. I. A. Wilson, J. J. Skehel, D. C. Wiley, Structure of the haemagglutinin membrane glycoprotein of influenza virus at 3 Å resolution. *Nature* **289**, 366–373 (1981). Medline doi:10.1038/289366a0

67. Y. Okuno, Y. Isegawa, F. Sasao, S. Ueda, A common neutralizing epitope conserved between the hemagglutinins of influenza A virus H1 and H2 strains. *J. Virol.* **67**, 2552–2558 (1993). Medline

68. D. C. Ekiert, R. H. Friesen, G. Bhabha, T. Kwaks, M. Jongeneelen, W. Yu, C. Ophorst, F. Cox, H. J. Korse, B. Brandenburg, R. Vogels, J. P. Brakenhoff, R. Kompier, M. H. Koldijk, L. A. Cornelissen, L. L. Poon, M. Peiris, W. Koudstaal, I. A. Wilson, J. Goudsmit, A highly conserved neutralizing epitope on group 2 influenza A viruses. *Science* **333**, 843–850 (2011). Medline doi:10.1126/science.1204839